# Multifactorial causal model of brain (dis)organization and therapeutic intervention: Application to Alzheimer's disease

Yasser Iturria-Medina[a,b,*], Félix M. Carbonell[c], Roberto C. Sotero[d], Francois Chouinard-Decorte[a,b], Alan C. Evans[a,b], for the Alzheimer's Disease Neuroimaging Initiative[1]

[a] Montreal Neurological Institute, McGill University, Montreal, Canada
[b] Ludmer Centre for NeuroInformatics and Mental Health, Montreal, Canada
[c] Biospective Inc., Montreal, Canada
[d] Department of Radiology and Hotchkiss Brain Institute, University of Calgary, Canada

## ARTICLE INFO

## ABSTRACT

Generative models focused on multifactorial causal mechanisms in brain disorders are scarce and generally based on limited data. Despite the biological importance of the multiple interacting processes, their effects remain poorly characterized from an integrative analytic perspective. Here, we propose a spatiotemporal multifactorial causal model (MCM) of brain (dis)organization and therapeutic intervention that accounts for local causal interactions, effects propagation via physical brain networks, cognitive alterations, and identification of optimum therapeutic interventions. In this article, we focus on describing the model and applying it at the population-based level for studying late onset Alzheimer's disease (LOAD). By interrelating six different neuroimaging modalities and cognitive measurements, this model accurately predicts spatiotemporal alterations in brain amyloid-β (Aβ) burden, glucose metabolism, vascular flow, resting state functional activity, structural properties, and cognitive integrity. The results suggest that a vascular dysregulation may be the most-likely initial pathologic event leading to LOAD. Nevertheless, they also suggest that LOAD it is not caused by a unique dominant biological factor (e.g. vascular or Aβ) but by the complex interplay among multiple relevant direct interactions. Furthermore, using theoretical control analysis of the identified population-based multifactorial causal network, we show the crucial advantage of using combinatorial over single-target treatments, explain why one-target Aβ based therapies might fail to improve clinical outcomes, and propose an efficiency ranking of possible LOAD interventions. Although still requiring further validation at the individual level, this work presents the first analytic framework for dynamic multifactorial brain (dis)organization that may explain both the pathologic evolution of progressive neurological disorders and operationalize the influence of multiple interventional strategies.

## Introduction

Brain disorders are thought to be caused by multiple concomitant factors (Sheikh et al., 2012). In most typical generative models of brain dynamics and disease progression, neuronal function or misfolded protein alterations are considered to take action locally and spread through anatomical connections (Cabral et al., 2012; Friston et al., 2014; Iturria-Medina et al., 2014; Mišić et al., 2015; Raj et al., 2012; Sanz Leon et al., 2013; Sanz-Leon et al., 2015; Sotero et al., 2007; Stam et al., 2016; Valdes-sosa et al., 2011a). However, consistent evidence supports that other complex multifactorial mechanisms present major pathological roles (Bero et al., 2011; Crossley et al., 2014; Iturria-Medina and Evans, 2015; Schwarz and et al., 2004; Wu et al., 2016). For example, in the context of neurodegeneration, neuronal structural degeneration can trigger functional hyperexcitability, being an important cellular pathomechanism underlying network dysfunction (Šišková et al., 2014). Cerebral blood flow (CBF) dysregulation decouples energy supply and neural function (Andreone et al., 2015). Vascular dysregulation can also impact amyloid-ß (Aβ) clearance, due to the fact that Aβ efflux across the brain blood barrier (BBB)

---

sequestrates Aβ proteins (Qosa et al., 2014). Aβ increase has a negative impact on mitochondrial function, which can increase reactive oxygen species (ROS) production and alter brain metabolism, reducing also mitochondrial Aβ clearance in a continuous feed-forward mechanism (Readnower et al., 2011). Similarly, functional connections to Aβ binding areas explain the spatial mismatch between regional metabolic alterations and toxic Aβ presence (Klupp et al., 2014). These interactions reflect that the direct coupling among multiple biological factors is a key feature of the brain, both in health and disease. Nevertheless, despite the biological importance of the multifactorial interacting mechanisms, their effects remain poorly characterized from an integrative analytical perspective. This traditional lack of quantitative multifactorial causal models is a central obstacle to the identification of disease-specific triggering pathological events and the development of effective therapeutic treatments.

Correspondingly, we also continue to lack the analytical models capable of predicting the multifactorial brain impact of specific therapeutic interventions. Some pioneering work towards characterizing the impact of functional stimulation therapies has been recently proposed (Betzel et al., 2016; Muldoon et al., 2016). However, such studies have only considered a single biological driver and/or target factor (i.e. functional activity), failing to quantify the therapeutic impacts of misfolded proteins, vascular, metabolic, and structural modifying therapies, or their concurrent impacts on associated cognitive states. Thus far, we could partially summarize current challenges on brain generative modeling according to three main points: i) no consideration of local multifactorial biological interactions, ii) no consideration of the concurrent spreading of multiple pathological effects across physical brain networks and, importantly, iii) an inability to predict in advance the multifactorial effects of either single-target or combinatorial intervention strategies.

Late-onset Alzheimer´s disease (LOAD), the most prevalent form of dementia (WHO, 2016), is one of the most challenging brain disorders from a multifactorial modeling perspective. Up to date, all observational (Jack et al., 2013, 2010) and data-driven (Donohue et al., 2014; Dukart et al., 2013; Fonteijn et al., 2012; Iturria-Medina et al., 2016; Young et al., 2014) models that define a multifactorial LOAD pathogenesis are invariably based on the magnitude levels of the biomarkers, without accounting for the multiplicity of causal mechanisms that take place at different spatiotemporal scales (Iturria-Medina et al., 2016). Suffering also the limitations described above for typical generative causal models, LOAD studies lack a quantitative causal identification of the initial pathologic triggering events. Consequently, these studies also lack of effective therapeutic strategies, while the disease's worldwide impact continues to expand. Motivated by the current imperative need for identifying effective therapeutic agents for this disorder (Chen-Plotkin, 2014) and by the general lack of analytical brain multifactorial models, we propose here a 4D multifactorial causal model (MCM) of brain (dis)organization and cognition. Based on a multifactorial brain network formulation and the elements of the control theory (Kalman, 1963; Klickstein et al., 2016), this model accounts for regional multifactorial causal interactions, pathological propagations through physical networks (e.g. axonal and vascular connectomes), the subsequent impact on cognitive integrity, and the identification and effectiveness assessment of either single-target or combinatorial therapeutic interventions. The MCM considers that once a factor-specific event occurs in a given brain region or in a set of regions, it can directly interact with other biological factors and alter their states. The alterations can also spread through anatomical and vascular connections to other brain areas, where similar factor-factor and propagation mechanisms may occur, in a continuous cycle.

At the population-based level, we found that the MCM is able to accurately explain/predict multifactorial LOAD alteration patterns and clarify the disease-triggering pathological mechanisms. Our causal analysis suggests that an initial vascular disequilibrium in specific brain areas (e.g. hippocampus and entorhinal regions) may be the most-likely event triggering LOAD progression (Iadecola, 2004; Zlokovic, 2011). This may be explained by the high vulnerability/ fragility of the vascular system, which we found to be strongly influenced by other biological factors (i.e. glucose metabolism and structural degeneration). Our results also highlight the critical role of multiple factor-factor interactions, supporting that LOAD is a complex multifactorial process, where each biological factor has a key role on disease progression. When used here as an in silico evaluator of interventional treatments, the MCM provides evidence for the strategic importance of creating effective combinatorial therapies and the crucial need for considering multiple brain factors as endpoints, instead of merely cognitive biomarkers. It also provides an efficiency ranking of multiple possible LOAD interventions, which might explain why recent one-target Aβ based therapies failed to improve clinical outcomes in LOAD (Doody et al., 2014; Salloway et al., 2014). Finally, we emphasize that the proposed model and associated controllability/ therapeutic analysis are potentially extendable and applicable to numerous brain disorders. This further offers hope towards the assisted personalized intervention of brain pathologies, based on the computational characterization and controlling of individual multifactorial mechanisms at multiple spatiotemporal scales, from local neuronal circuits to macroscopic brain networks.

## Methods

### Ethics statement

The study was conducted according to Good Clinical Practice guidelines, the Declaration of Helsinki, US 21CFR Part 50 – Protection of Human Subjects, and Part 56 – Institutional Review Boards, and pursuant to state and federal HIPAA regulations (adni.loni.usc.edu). Study subjects (Table S1) and/or authorized representatives gave written informed consent at the time of enrollment for sample collection and completed questionnaires approved by each participating site Institutional Review Board (IRB). The authors obtained approval from the ADNI Data Sharing and Publications Committee for data use and publication, see documents http://adni.loni.usc.edu/wp-content/uploads/how_to_apply/ADNI_Data_Use_Agreement.pdf and http://adni.loni.usc.edu/wp-content/uploads/how_to_apply/ADNI_Manuscript_Citations.pdf, respectively.

### Data description and processing

#### Study participants

This study used 561 individual baseline data from the Alzheimer's Disease Neuroimaging Initiative (ADNI) (adni.loni.usc.edu). At least three different imaging modalities were acquired for each included subject (i.e. structural MRI, Fluorodeoxyglucose PET, resting Functional MRI, Arterial Spin Labeling and/or Amyloid-ß PET). The ADNI was launched in 2003 as a public-private partnership, led by Principal Investigator Michael W. Weiner, MD. The primary goal of ADNI has been to test whether serial magnetic resonance imaging (MRI), positron emission tomography (PET), other biological markers, and clinical and neuropsychological assessments can be combined to measure the progression of mild cognitive impairment (MCI) and early Alzheimer's disease (AD).

See Table S1 for demographic characteristics of the included ADNI subjects.

#### Structural MRI acquisition/processing

Brain structural T1-weighted 3D images were acquired for all subjects. For a detailed description of acquisition details, see http://adni.loni.usc.edu/methods/documents/mri-protocols/. All images underwent non-uniformity correction using the N3 algorithm (Sled et al., 1998). Next, they were segmented into grey matter, white matter and cerebrospinal fluid (CSF) probabilistic maps, using SPM12 (www.

fil.ion.ucl.ac.uk/spm). Grey matter segmentations were standardized to MNI space (Evans et al., 1994) using the DARTEL tool (Ashburner, 2007). Each map was modulated in order to preserve the total amount of signal/tissue. Mean grey matter density and determinant of the Jacobian (DJ) (Ashburner, 2007) values were calculated for 78 regions covering all the brain's grey matter (Klein and Tourville, 2012). For each region, obtained grey matter density and DJ values were statistically controlled for differences in acquisition protocols. Both measurements provided equivalent modeling results. All the results/figures presented in this study correspond to the DJ, which constitutes a robust local measure of structural atrophy.

*Fluorodeoxyglucose PET acquisition/processing*

A 185 MBq (5+0.5 mCi) of [18F]-FDG was administered to each participant and brain PET imaging data were acquired approximately 20 min post-injection. All images were corrected using measured attenuation. Also, images were preprocessed according to four main steps (Jagust et al., 2010): 1) dynamic co-registration (separate frames were co-registered to one another lessening the effects of patient motion), 2) across time averaging, 3) re-sampling and reorientation from native space to a standard voxel image grid space ("AC-PC" space), and 4) spatial filtering to produce images of a uniform isotropic resolution of 8 mm FWHM. Next, using the registration parameters obtained for the structural T1 image with nearest acquisition date, all FDG-PET images were spatially normalized to the MNI space (Evans et al., 1994). Regional standardized uptake value ratio (SUVR) values for the 78 regions considered (Klein and Tourville, 2012) were calculated using the cerebellum as reference region.

*Resting fMRI acquisition/processing*

Resting-state functional images were obtained using an echo-planar imaging sequence on a 3.0-Tesla Philips MRI scanner. Acquisition parameters were: 140 time points, repetition time (TR)=3000 ms, echo time (TE)=30 ms, flip angle=80°, number of slices=48, slice thickness=3.3 mm, spatial resolution=3×3×3 mm$^3$ and in plane matrix=64×64. Preprocessing steps included: 1) motion correction, 2) slice timing correction, 3) spatial normalization to MNI space (Evans et al., 1994) using the registration parameters obtained for the structural T1 image with the nearest acquisition date, and 4) signal filtering to keep only low frequency fluctuations (0.01−0.08 Hz) (Chao-Gan and Yu-Feng, 2010). In order to have regional quantitative indicators of the brain's functional integrity, fractional amplitude of low-frequency fluctuation (fALFF) (Zou et al., 2008), regional homogeneity (ReHo) (Zang et al., 2004), and functional connectivity degree (van den Heuvel and Hulshoff Pol, 2010) measures were calculated for each considered brain region. Among these three measurements, fALFF showed the highest sensibility to disease progression (Iturria-Medina et al., 2016). Consequently, all the analyses and results presented in this study correspond to this measure.

*ASL acquisition/processing*

Resting Arterial Spin Labeling (ASL) data were acquired using the Siemens product PICORE sequence. Acquisition parameters were: TR/TE=3400/12 ms, TI1/TI2=700/1900 ms, FOV=256 mm, 24 sequential 4 mm thick slices with a 25% gap between the adjacent slices, partial Fourier factor=6/8, bandwidth=2368 Hz/pix, and imaging matrix=64×64. For preprocessing details see "UCSF ASL Perfusion Processing Methods" in www.adni.loni.usc.edu. In summary, main preprocessing steps included: 1) motion correction, 2) perfusion-weighted images (PWI) computation, 3) intensity scaling, 4) CBF images calculation, 5) spatial normalization to MNI space (Evans et al., 1994) using the registration parameters obtained for the structural T1 image with the nearest acquisition date, and 6) mean CBF calculation for each considered brain region.

*Amyloid-β PET acquisition/processing*

A 370 MBq (10 mCi ± 10%) bolus injection of AV-45 was administered to each participant, and 20 min continuous brain PET imaging scans were acquired approximately 50 min post-injection. The images were reconstructed immediately after the 20 min scan, and when motion artifact was detected, another 20 min continuous scan was acquired. For each individual PET acquisition, images were initially preprocessed according to four main steps (Jagust et al., 2010): 1) dynamic co-registration (separate frames were co-registered to one another lessening the effects of patient motion), 2) across time averaging, 3) re-sampling and reorientation from native space to a standard voxel image grid space ("AC-PC" space), and 4) spatial filtering to produce images of a uniform isotropic resolution of 8 mm FWHM. Next, using the registration parameters obtained for the structural T1 image with the nearest acquisition date, all amyloid images were spatially normalized to the MNI space (Evans et al., 1994). Considering the Cerebellum as an Aß non-specific binding reference, SUVR values for the 78 grey matter regions considered were calculated.

*Diffusion weighted MRI (DW-MRI) acquisition*

High angular resolution diffusion imaging (HARDI) data was acquired for 225 subjects. For each diffusion scan, 46 separate images were acquired, with 5 $b_0$ images (no diffusion sensitization) and 41 diffusion-weighted images ($b$=1000 s/mm$^2$). Other acquisition parameters were: 256×256 matrix, voxel size: 2.7×2.7×2.7 mm$^3$, TR=9000 ms, 52 contiguous axial slices, and scan time 9 min. ADNI aligned all raw volumes to the average b0 image, corrected head motion and eddy current distortions. See *Multimodal connectivity estimation* subsection for anatomical network reconstruction details.

*Data quality control and clinical homogenization*

In order to control for possible noise and heterogeneity effects, before model fitting and evaluations we performed a robust data homogeneity/quality control, consisting of two main steps (described previously in (Iturria-Medina et al., 2016)):

 i) Calculation of individual likelihood scores reflecting how accurately each subject was diagnosed by the clinical experts, and subsequent elimination of the subjects with low likelihood scores (below the 10th percentile).
 ii) For each biomarker and clinical group, outlier identification was performed based on the Mahalanobis distance (Wilks, 1966), with a significative squared distance (P < 0.05) meaning an outlier (for implementation details, see (Trujillo-Ortiz et al., 2006)). Outlier detection for imaging biomarkers considered all brain regions, using the multivariate Mahalanobis distance.

Step (i) controlled for cognitive heterogeneity, whereas (iii) controlled for variability and noise on biological measurements, improving both cognitive and biological data homogeneity at the clinical group levels.

*Multimodal connectivity estimation*

*Vascular Networks*

For each clinical group, direct region-region vascular connectivity measurements, in the range $C_{j \to i}^{vasc} \in [0,1]$, were obtained using tree-based ensemble Random Forests (Huynh-Thu et al., 2010) and the preprocessed/regional CBF data. This algorithm, known as GENIE3, is commonly employed to reconstruct direct gene regulatory networks, demonstrating high predictive accuracy and outperforming other popular connectivity methods on both synthetic and real data. GENIE3 decomposes the prediction of a direct network between $N$ nodes (brain regions) into $N$ different hierarchical regression problems, and reduces the number of possible interactions (possible predictors of each node) based on an automatic feature selection with tree-based

ensemble methods. It is a generic algorithm, adaptable to different types of associative data and linear/nonlinear interactions (Huynh-Thu et al., 2010). Due to the statistical nature of the GENIE3 algorithm, the obtained vascular networks would be reflecting covariance patterns among the regions, similarly to functional and structural networks created via association techniques (Evans, 2013; Monti et al., 2014; van den Heuvel and Hulshoff Pol, 2010). However, a crucial distinction is that GENIE3 controls for indirect relationships among the nodes, providing only the statistical evidence/likelihood supporting each potential direct vascular interaction.

*Anatomical Networks*

Probabilistic axonal connectivity values between each brain voxel and the surface of each considered gray matter region (voxel-region connectivity) were estimated using a fully automated fiber tractography algorithm (Iturria-Medina et al., 2007) and the intravoxel fiber distributions (ODFs) of 225 healthy and diseased subjects from ADNI (Table S1). ODF reconstructions were based on Spherical Deconvolution (Tournier et al., 2008). A maximum of 500 mm trace length and a curvature threshold of $\pm 90°$ were imposed as tracking parameters. Based on the resulting voxel-region connectivity maps, the individual region-region anatomical connection density matrices (Iturria-Medina et al., 2007) were calculated. For any subject and pair of regions $i$ and $j$, the $ACD_{i,j}$ measure ($0 \le ACD_{i,j} \le 1$, $ACD_{ij} \equiv ACD_{ji}$) reflects the fraction of the region's surface involved in the axonal connection with respect to the total surface of both regions. For each clinical state *clin*, we calculated its characteristic anatomical network $C_{j\to i}^{anat}$ as the average $ACD$ matrix from the subjects at that clinical state.

Finally, the (dis)similarity between the reconstructed vascular and anatomical networks was evaluated via a Mantel test with permutations. For associated results, see *Characterizing direct factor-factor interactions and intra-brain propagation properties* subsection.
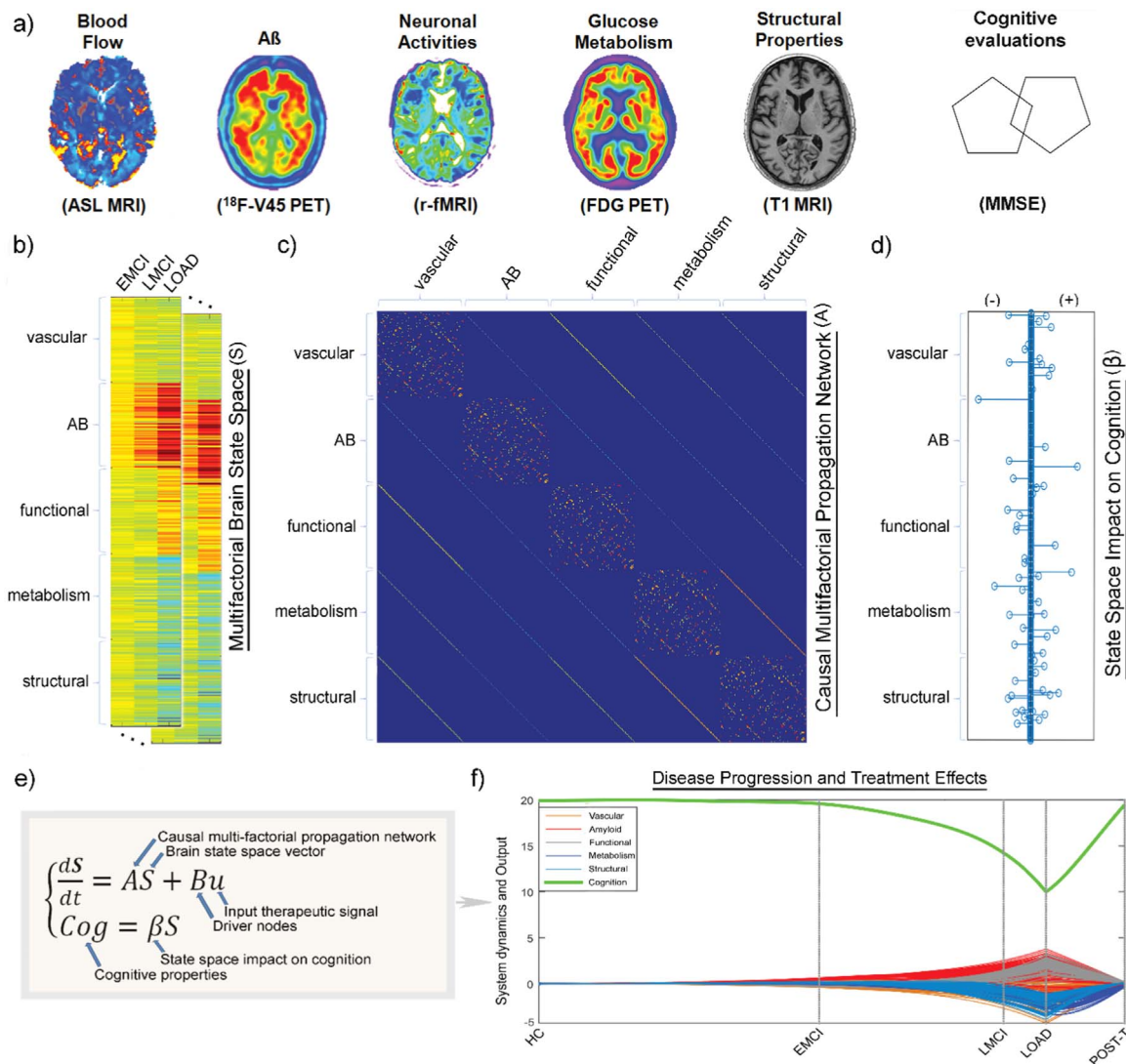


**Fig. 1.** Representation of the MCM approach. a) Brain multimodal images and cognitive evaluation used in this study. b) State space vectors (*S*), characterizing the brain's multifactorial alteration/disequilibrium levels with regard to a baseline, across regions and at different disease stages. Here, we used the average data of the clinically normal subjects to define the initial baseline. The alteration/disequilibrium levels are calculated then as the standardized difference with the baseline. c) Causal multifactorial propagation network (matrix *A*, see *Methods and Text S1*) capturing the direct interactions among regions (for each biological factor/imaging modality) or among factors (for each brain region). Diagonal blocks in *A* correspond to a unique biological factor, with diagonal elements accounting for intraregional effects (e.g. local regional balance among: functional hyper excitation and inhibition, production and degradation of misfolded proteins, or proliferation and restoration of damaged tissue properties) and off-diagonal elements accounting for interregional alterations spreading across physical connections. Off-diagonal blocks in *A* correspond to the direct interactions among two different factors (e.g. glucose metabolism impact on tissue properties, or vice versa). d) System's output vector (*β*), representing the influence of the brain's multifactorial state space on the cognitive state (for obtained values, see Table S3 and Fig. S3). e) Conceptual MCM. f) Reconstructed multimodal trajectories after introducing an initial alteration in a specific brain region and factor, followed by a hypothetical low-cost input therapeutic signal (*u*). Notice the strong cognitive deterioration with disease progression, from transition HC to LOAD, and how it is recovered at the hypothetical post-treatment (POST-T) point. See also Videos S1–S5 and Figs. 7, 8. For visualization purposes, in (f) the cognitive variable was rescaled to the range [10-20].

## Multifactorial causal model of brain (dis)organization and therapeutic intervention

Here we consider the brain as a dynamic multifactorial causal system, where: i) each system node (or variable) models a relevant biological factor at a given brain region, and ii) alterations in each biological factor are caused by direct factor-factor interactions and/or external inputs. For example, in the context of our LOAD study, we consider $N_{factors}$=5 different biological factors (i.e. vascular flow, Aß deposition, glucose metabolism, functional activity at rest, and gray matter density), each measured at $N_{rois}$=78 different brain regions of interest (Klein and Tourville, 2012) covering all the brain's gray matter (see Fig. 1). Each node, corresponding to a given biological factor $m$ and region $i$, is characterized by its alteration/disequilibrium level, $S_i^m \in \mathbb{R}$, reflecting the dissimilarity/distance to an initial state ($S_i^m$=0, $S_i^m$<0, or $S_i^m$>0 indicating non alteration, decrease, or increment with regard to baseline, respectively). Also, to model the direct coupling between all factors, the system is characterized by a *dynamic multifactorial direct interaction network* ($A$), where each directed edge corresponds to a factor-factor interaction (for schematic representation, see Fig. 1c; for biological examples, see first paragraph of *Introduction* and third-fourth paragraphs of *Discussion*). In summary, at each time point the described brain system is defined by the [$N_{factors}N_{rois}$x1] state space vector $S(t)=[S_1^1(t), S_2^1(t), ..., S_i^m(t), ..., S_{Nrois}^{N_{factors}}(t)]^T$ and $A(t)$ (Fig. 1b–c).

In the absence of external inputs, the dynamic behavior of the proposed brain system will depend only on the direct interactions among its nodes, which are defined by: (i) the local direct interactions among all the biological factors, constrained within each brain region, (ii) the potential propagation of factors-specific alterations through "physical" networks (i.e. anatomical and/or vascular networks), and (iii) the preservation, during the propagation processes, of the new generated intra-factorial alterations. These processes can be described by the differential equation model:

$$\frac{dS_i^m}{dt} = \sum_{n=1}^{N_{factors}} \alpha^{n \to m} S_i^n + \sum_{\substack{j=1, \\ j \neq i}}^{N_{rois}} C_{j \to i}^m(t) S^m S_j^m - \sum_{\substack{j=1, \\ j \neq i}}^{N_{rois}} C_{i \to j}^m(t) S^m S_i^m. \quad (1)$$

The first term ($\sum_{n=1}^{N_{factors}} \alpha^{n \to m} S_i^n$), models the local direct influences of multiple biological factors on the given factor $m$. $\alpha^{n \to m}$ is the interaction parameter controlling the direct intra-regional impact of the factor $n$ over factor $m$, including intra-factor effects (i.e. $n = m$). Note that these interactions occur only inside each brain region, without mediation of inter-regional effects (for biological examples, see first paragraph of *Introduction* and third-fourth paragraphs of *Discussion*).

The second term ($\sum_{\substack{j=1, \\ j \neq i}}^{N_{rois}} C_{j \to i}^m(t) S^m S_j^m$), models the changes in $S_i^m$ due to the input of signals of the same factor $m$, from other physically connected brain regions. This propagation can occur through the anatomical and/or vascular connectomes, depending of the spreading mechanisms associated each biological factor. For example, a vascular alteration should propagate mostly, if not entirely, by the brain's vascular network, while the Aß proteins may propagate through both the anatomical and the vascular networks (Iturria-Medina et al., 2014; Qosa et al., 2014). In order to capture the multiplicity of different spreading mechanisms, for each factor $m$ we define its characteristic dynamic multimodal network (with connection value $C_{j \to i}^m(t)$, for each pair of brain regions $j$ and $i$). This factor-specific network reflects how much the alterations in factor $m$ propagate from region $j$, by the vascular and/or the anatomical networks, to impact the same factor $m$ at region $i$, allowing the estimation of the fraction that propagates by one or the other connectional substrate. Consequently, for each factor $m$ the corresponding dynamic multimodal network is defined as the weighted combination:

$$C_{j \to i}^m(t) = w^m C_{j \to i}^{vasc}(t) + (1 - w^m) C_{j \to i}^{anat}(t), \quad (2)$$

where $w^m \in [0,1]$ is the fraction of the propagation (of factor $m$) that spread through the vascular connection ($C_{j \to i}^{vasc}(t)$) and $(1 - w^m)$ is the remaining fraction that spread through the anatomical connection ($C_{j \to i}^{anat}(t)$). $S^m$>0 is a propagation weight parameter for each factor $m$, reflecting the factor's global tendency to spread through brain connections. See *Multimodal connectivity estimation* subsection (above) for details about the vascular/anatomical network construction.

The last term ($\sum_{\substack{j=1, \\ j \neq i}}^{N_{rois}} C_{i \to j}^m(t) S^m S_i^m$), reflects the amount of signal for factor $m$ that propagates from region $i$ to all other brain regions, through factor $m$'s characteristic dynamic multimodal network. The addition of this term guarantees the instantaneous preservation of the new alterations generated in each region $i$. Once an increment or decrease occurs in the alteration/disequilibrium level of factor $m$ at region $i$, this alteration can partially or totally propagate to other brain regions, depending of factor $m$'s propagation capacity and the multimodal connectional pattern of region $i$ (reflected in $S^m$ and $C_{i \to j}^m$, respectively). Thus, it is necessary to discount the alteration level that is leaving region $i$.

In addition, in order to capture cognitive ($Cog$) alterations associated with pathological progression, the expression (1) is accompanied by the algebraic expression:

$$Cog(t) = \beta_0^{cog} + \sum_{m=1}^{N_{factors}} \sum_i^{N_{rois}} \beta_i^{m,cog} S_i^m(t). \quad (3)$$

$Cog$ is modeled by additive linear relationships, considering the brain's multifactorial alterations as modulators. Both expressions (1) and (3) describe the brain's dynamic and cognitive state, and they can be rewritten in vector form by the linear dynamic system:

$$\begin{cases} \frac{dS}{dt} = A(t)S, \\ Cog = \beta S, \end{cases} \quad (4)$$

where $A(t)$ is the *dynamic multifactorial direct interaction network*, which as previously mentioned defines the complex dynamic of the brain system (see Fig. 1c). It is a [$N_{factors}N_{rois} \times N_{factors}N_{rois}$] asymmetric matrix characterizing all the multifactorial interactions at time $t$. It depends on the model parameters ($\alpha^{n \to m}$, $S^m$, $w^m$) which are estimated during model fitting, and also on the brain's connection properties ($C_{i \to j}^m(t)$), estimated a priori. See Text S1 for the explicit analytical expression of $A(t)$. $\beta = [\beta_0^{cog}...\beta_{N_{rois}}^{N_{factors},cog}]^T$ is the system's output vector, which define the relation between the state space ($S$) and the cognitive state. All $\beta$ coefficients in (3 and 4) correspond to fixed effects across the entire population and are estimated a priori using a robust linear regression algorithm (Street et al., 1988). The initial condition of this system, $S(t_0)$ and $Cog(t_0)$, define the multifactorial alteration/disequilibrium level and cognitive properties at the initial time point of interest for the modeling process ($t_0$). In this study, $t_0$ is assumed as the disease onset time, at which a regionally localized deviation from a theoretical pathology-free state starts.

To account for external inputs on the introduced brain dynamic system, according to control theory (Kalman, 1963; Liu et al., 2011), expression (4) can be extended as:

$$\begin{cases} \frac{dS}{dt} = A(t)S + Bu, \\ Cog = \beta S, \end{cases} \quad (5)$$

where $B$ is an [$N_{factors}N_{rois}$x$M$] input matrix ($M \leq N_{factors}N_{rois}$) that identifies $M$ nodes (brain regions of any specific biological factor or factors) controlled by an outside controller (Kalman, 1963; Liu et al., 2011). $u(t)=[u_1(t)...u_M(t)]$ is the associated time-dependent input signal.

In the context of neurological disorders, an effective therapeutic treatment should drive the patient from an abnormal cognitive/clinical state ($Cog_0$) to a final normal state ($Cog_f$). In order to accomplish this, we will explore two different controlling strategies: i) *output control strategy*, focusing mostly in the control of the system's cognitive

output, and ii) *full control strategy*, focusing in the control of every state node, which indirectly will modify the system's output. For the *output control strategy*, the reduction on the number of target variables can substantially decrease the amount of driver nodes and control energy, particularly in comparison to the full network control case (Gao et al., 2014; Klickstein et al., 2016). Thus, for each hypothetical set of controlling nodes $B$, if we consider a given time period with constant (or approximately constant) causal network matrix $A$, the optimum input signal to minimize the output control energy can be estimated as (Klickstein et al., 2016):

$$u_{opt}^{Cog_0 \to Cog_f}(t) = -B^T e^{A^T(t_f - t)} \beta^T (\beta W \beta^T)^{-1} D, \tag{6}$$

where $W$ is the controllability gramian matrix (Kailah, 1980):

$$W(t_0, t_f) = \int_{t_0}^{t_f} e^{A(t_0 - t)} B B^T e^{A^T(t_0 - t)} dt, \tag{7}$$

and $D = (\beta e^{A(t_f - t)} S(t_0) - Cog_f)$ is the difference between the desired final and the final output under the free evolution. For the *full control strategy*, the optimum input signal can be estimated as (Klickstein et al., 2016):

$$u_{opt}^{S_0 \to S_f}(t) = -B^T e^{A^T(t_f - t)} W^{-1} D, \tag{8}$$

being $D = (e^{A(t_f - t)} S(t_0) - S(t_f))$ the difference between the final and desired final state space vector under the free and controlled evolution, respectively.

Finally, for each controlling strategy, the cost-energy function associated to the set of nodes $B$ with optimum strategy $u_{opt}$ (i.e. $u_{opt}^{Cog_0 \to Cog_f}$ or $u_{opt}^{S_0 \to S_f}$) is:

$$J(B, u_{opt}) = \int_{t_0}^{t_f} (u_{opt}(t))^T u_{opt}(t) dt. \tag{9}$$

See Text S1 for the explicit analytical expression of $A(t)$, Text S2 for model optimization algorithm, and following subsections for model interpretation and evaluation details.

*Interpreting factor-factor direct interactions and alteration spread*

As mentioned, the *dynamic multifactorial direct interaction network* $A(t)$ defines the complex dynamic of the brain system. Thus, the characterization and interpretation of this network, in biological terms, is crucial for understanding the complex mechanisms underlying a given brain (dis)organization process. However, due to the arbitrary scale of the interaction and spreading parameters ($\alpha^{n \to m}$ and $S^m$ coefficients), the comparison and interpretation requires an appropriate normalization procedure, correcting for all possible interactions/spreading effects in the multifactorial network. To accomplish this, here we defined four different measures:

The *relative factor-factor influence* $I(n \to m)$ reflects the percent of regional changes in factor $m$ that are caused by the direct influence of factor $n$. It is calculated as the sum of the direct effects of $n$ over $m$, across all brain regions (reflected in the $\alpha^{n \to m}$ coefficient), relative to the total direct effects of all the biological factors over $m$, including self-effects. Mathematically:

$$I(n \to m) = 100 * \int_{t_0}^{t} \frac{\alpha^{n \to m} N_{rois}}{\sum_{k=1}^{N_{factors}} \alpha^{k \to m} N_{rois} + S^m \sum_{i,j,i \neq j}^{N_{rois}} C_{i \to j}^m(t)} dt. \tag{10}$$

The *relative outgoing influence* $I(n \to)$, similar to the out-strength measure in a directed network (see Rubinov and Sporns, 2010), reflects the percent of regional changes in all the considered biological factors that are caused by the direct influence of a given biological factor $n$, excluding self-effects. This measure can be particularly useful to detect the most influential biological factors during a brain process.

The *relative incoming influence* $I(m \leftarrow)$, similar to the in-strength measure in a directed network (Rubinov and Sporns, 2010), reflects the percent of regional changes in factor $m$ that are caused by the direct

influences of all the other biological factors, excluding self-effects. This measure allows the identification of the most vulnerable and influenced biological factors during a given brain process.

Finally, the *relative spreading* $Diff(m)$ reflect the percent of the regional changes in factor $m$ that are caused by intra-factor spreading through the brain's physical connections. Mathematically:

$$Diff(m) = 100 * \int_{t_0}^{t} \frac{S^m \sum_{i,j,i \neq j}^{N_{rois}} C_{i \to j}^m}{\sum_{k=1}^{N_{factors}} \alpha^{k \to m} N_{rois} + S^m \sum_{i,j,i \neq j}^{N_{rois}} C_{i \to j}^m(t)} dt. \tag{11}$$

*Model evaluation and validation with real data*

*Disease progression analysis*

First, we aimed to reproduce and predict the characteristic multi-factorial alteration patterns of LOAD evolution. The analysis consisted of introducing a small alteration at a hypothetical free-pathology state, modeling an initial disease triggering event, and evaluating the model's accuracy to explain or predict the imaging and cognitive data available for all the subjects at early mild cognitive impairment (EMCI), late mild cognitive impairment (LMCI), and LOAD states, guaranteeing the spatiotemporal continuity across clinical transitions. Before model fitting and evaluations, all considered imaging and cognitive descriptors were previously controlled for age, gender, number of apoeε4 allele copies, educational level and all their possible pairwise interactions. Also, in order to control for possible noise and heterogeneity effects, we performed a robust data homogeneity/quality control, consisting of two main steps that controlled for variability and noise in measurements, improving both biological and cognitive data homogeneity at the clinical group levels (see *Data quality control and clinical homogenization* subsection). Then, all subjects were aligned according to their clinical state, obtaining a multimodal sample in which the individual observations are ordered in terms of disease severity, and covering the whole LOAD evolution.

Notice that in the case of an analysis based in disease evolution, the time variable in (1–9) loses its "aging" interpretation. The time component is relevant only for the individual cases and at the group level this variable should be interpreted instead in terms of disease progression. Consequently, in this case the time variable ($t$) was replaced by a continuous disease progression variable ($DP \in [0,1]$), assuming $DP = 0$ for an ideal clinically normal state (HC) and $DP = 1$ for the most advanced disease state (LOAD). $DP$ values for EMCI and LMCI ($DP^{EMCI}$ and $DP^{LMCI}$, respectively) are estimated automatically by the model´s optimization algorithm (see below and Text S2). As all the biological/cognitive descriptors were previously controlled by age and its interactions with the other demographic variables, the use of the $DP$ variable as the progressive component in the model enables focusing on the multivariate changes directly associated to the pathologic evolution, without the confounding effects of the temporal/aging process.

Then, for each factor $m$, brain region $i$, and subject $k$ at the disease progression state $DP$, we calculated its alteration level as the deviation from the characteristic clinically normal state:

$$S_{k,i}^m(DP) = (x_{k,i}^m(DP) - \mu_i^m(HC)), \tag{12}$$

where $x_{k,i}^m(DP)$ is the observed individual value, and $\mu_i^m(HC)$ is the mean value observed for the clinically normal group, respectively, after controlling for the mentioned covariables and all their possible pairwise interactions. Importantly, in order to make the alteration patterns and their associated model parameters comparable across all imaging modalities, for each imaging modality, all alteration levels were standardized to have standard deviation 1 across subjects and regions.

It is important to consider that, for a discrete number of possible clinical states $N_{clin}$ (i.e. *clin=1.4*, corresponding to HC, EMCI, LMCI and LOAD clinical states respectively), after substituting the time

variable ($t$) by the disease progression variable ($DP$), the state space system in (1, 3 and 5) has the following analytical solution:

$$S(DP) = \left( \prod_{DP_{clin}=1}^{DP_{clin}=N_{clin}} e^{A(DP) \cdot (DP - DP_{clin-1})} \right) S(DP_0).$$

(13)

$DP_0$ is the disease onset point, at which the regionally localized deviation from a theoretical pathology-free state starts. In this case, the model's optimization function is:

$$\mathcal{L}(\varnothing) = \sum_{DP_{clin}=1}^{DP_{clin}=N_{clin}} \left( \sum_{m=1}^{N_{factors}} \sum_{i=1}^{N_{rois}} \frac{1}{N_m} \sum_{s=1}^{N_m} (S_{k,i}^m(DP) - \hat{S}_i^m(DP; \varnothing)) \right)^2,$$

(14)

where $N_m$ is the number of subjects with available data for the biological factor $m$. $\hat{S}_i^m(DP; \varnothing)$ is the estimated alteration level for factor $m$ and brain region $i$, at the disease state $DP$, for the set of model parameters $\varnothing$.

Next, all the biological factors ($m=1.5$) and brain regions (i.e. a total of $5 \cdot 78 = 390$, for the used five imaging modalities and brain parcellation), were explored as possible candidates (causal epicenters) to start the LOAD pathologic process. For this, we defined a novel optimization algorithm (see Text S2) that allows the estimation of the optimum initial pathologic perturbation (S($DP_0$)), and the corresponding model parameters ($\varnothing = [\alpha^{n \to m} S^m w^m DP^{EMCI} DP^{LMCI}]$, for $n,m=1:5$) that better explain (minimizing expression (11)) the reference alteration patterns across all the subjects and the three different clinical states (EMCI, LMCI, LOAD). The two steps optimization was performed using a least squares regularization method (Tibshirani, 1996) and the trust-region-reflective least squares algorithm (Coleman and Li, 1996, 1992), implemented in the MATLAB functions lasso and lsqnonlin, respectively.

*Model cross-validation*

In order to evaluate the MCM's predictive power on new instances of data, we first used the multifactorial alteration patterns observed for subjects at EMCI and LMCI states to predict the future trajectories of the data, fitting the model with only these two states and projecting the alteration pattern at $DP=1$ (i.e. the disease progression state or time that a hypothetical subject should reach the LOAD stage). Secondly, we evaluated the model's capacity to predict the past trajectories of the data, fitting the model with the subjects at the LMCI and LOAD states and projecting (via backward integration) the alteration pattern at $DP = DP^{EMCI}$. Notice that, for this particular case, a high accuracy predicting the multifactorial alteration pattern for the EMCI stage (from the future instances of data) would be supporting also the validity of the estimated initial pathologic perturbation (S($DP_0$)), described in the previous subsubsection and Text S2. Finally, we repeated the same procedure but now using EMCI and LOAD subjects to predict the alteration patterns for LMCI subjects, evaluating the model's capacity to predict intermediary disease stages. For associated results, see *Reproducing and predicting multifactorial alteration patterns in LOAD progression* subsection.

*Most-likely disease triggering events and regional epicenters*

We used a bootstrapping procedure, creating $N_{boots}=500$ different data sets with replacement, and repeating the previous model optimization, to identify the most-likely/probable disease triggering factor(s) and associated regional epicenter(s), across all generated samples. For each factor $m$, its probability of being a potential triggering factor of the LOAD process was calculated as:

$$P^m(DP_0) = \frac{\sum_{b=1}^{N_{boots}} Factor^m(DP_0)}{N_{boots}},$$

(15)

where $Factor^m(DP_0)$ is a step function, reflecting if factor $m$ is altered or not, at least for one brain region, at the initial condition:

$$Factor^m(DP_0) = \begin{cases} 1, & if\, \hat{S}_i^m(DP_0) \neq 0 \quad for\, any\, region\, i\, (i=1:N_{rois}) \\ 0, & otherwise \end{cases}.$$

(16)

Similarly, for each brain region $i$, its probability of being a disease spatial epicenter, was calculated as:

$$P_i(DP_0) = \frac{\sum_{b=1}^{N_{boots}} Region_i(DP_0)}{N_{boots}},$$

(17)

with:

$$Region_i(DP_0) = \begin{cases} 1, & if\, \hat{S}_i^m(DP_0) \neq 0 \quad for\, any\, factor\, m\, (m=1:N_{factors}) \\ 0, & otherwise \end{cases}.$$

(18)

For associated results, see *Identifying potential triggering events in LOAD* subsection.

*Evaluating possible therapeutic impacts*

In order to evaluate the effectiveness of possible one-target or combinatorial therapies, for each biological factor or combination of three factors, we used expressions (5)–(9) to estimate the optimum input signal and cost-energy to minimize the control energy, during hypothetical LOAD to HC clinical transitions. For a single-target intervention, based in a unique driver factor, the input matrix $B$ (Eq. (5)) was constructed with one for all the nodes/regions corresponding to this factor, and zero for all the other nodes/regions. Similarly, for a combinatorial intervention, the matrix $B$ had one for all the nodes/regions associated to the selected driver factors and zero for the rest. For associated results, see the *Identifying optimum therapeutic strategies for stopping and reversing LOAD progression* subsection.

*Robustness to different brain parcellation schemes*

In order to explore the model´s robustness to different gray matter parcellation schemes, we repeated all the previous analyses for the AAL parcellation (Tzourio-Mazoyer et al., 2002), considering 90 cortical and subcortical areas covering all the brain´s gray matter. See the *Discussion* section (*Limitations and future work* subsection).

## Results

*Multifactorial causal model of brain (dis)organization and intervention*

We formulated a novel 4D spatiotemporal multifactorial causal model that accounts for multiple brain biological factors, cognitive changes and controllability properties (see *Methods*). By estimating the model's biological parameters, and performing a multifactorial controllability analysis, it is possible to obtain quantitative information about: (i) probable initial triggering events and associated "epicenter" brain regions associated to a given brain (dis)organization process, (ii) relative factor-factor direct interactions weights, (iii) relative vulnerability and influence level of each considered biological factor, (iv) relative level of intra-brain propagation of each biological factor's alteration/disequilibrium, as well as the corresponding fraction that propagates through specific physical networks (e.g. anatomical and/or vascular networks), (v) relative times among different clinical sub-stages of the disorder, and (vi) identification of optimum (i.e. low-cost) therapeutic strategies to stop/reverse multifactorial pathological processes.

*Reproducing and predicting multifactorial alteration patterns in LOAD progression*

We used the formulated model to investigate the mechanisms underlying LOAD development, progression and potential interventions. Similarly to a previous study (Iturria-Medina et al., 2016), we evaluated Aβ misfolded proteins, glucose metabolism, CBF, functional

activity in rest, and/or structural brain tissue patterns in a cohort of 561 subjects from the ADNI database (*Methods, Study participants*; Table S1). These five biological factors were mapped *in vivo* using advanced neuroimaging techniques (Fig. 1; *Methods, Data Description and Processing*). Each participant had been previously diagnosed at each visit as healthy control (HC), early mild cognitive impairment (EMCI), late mild cognitive impairment (LMCI) or probable Alzheimer's disease patient (LOAD). In addition, participants were cognitively characterised according to the Mini Mental State Examination (MMSE), which was used here as a measure of cognitive integrity. For each mentioned biological factor, representative regional values were calculated for 78 regions covering all the brain's grey matter (Klein and Tourville, 2012) (*Methods, Image processing* subsection). For each clinical group, each specific descriptor was compared with an age-matched clinically normal reference (see *Methods, Model evaluation and validation with real data*), obtaining an average distance-based score of disequilibrium/alteration compared to the healthy baseline. This calculation was repeated 500 times via a bootstrapping technique (with replacement), which improved the robustness of the estimations and allowed us to control the stability of the results.

Supplementary material related to this article can be found online at http://dx.doi.org/10.1016/j.neuroimage.2017.02.058.

Next, we evaluated the competence of the MCM to reproduce the observed EMCI, LMCI and LOAD multimodal imaging and cognitive alteration patterns, starting from a characteristic HC state. The analysis consisted of introducing a small pathologic alteration at the clinically normal state, modeling the initial disease triggering event, and evaluating the model's accuracy to reproduce the real diseased data. The statistical complexity of this analysis resides in the replication of the alteration values of $N_{factors}N_{rois}+1$ variables (the total number of regions for all biological factors plus one cognitive variable, i.e. 391), guaranteeing the spatiotemporal continuity across three different clinical states (i.e. a total of 391*3=1173 values) with a considerably smaller number of model parameters (i.e. 37 model parameters). A fully automated algorithm and a bootstrapping procedure were used to identify the most-likely pathological initial condition (i.e. the perturbation introduced at the clinically normal state) and to estimate the model's biological parameters. For estimation details, see *Methods, Model evaluation and validation with real data* subsection, and Text S2.

The results (Fig. 2a) demonstrate the MCM's capability to explain intermediate and advanced LOAD alterations. It explains 84.36% (P <

0.0001) of the variance in multifactorial regional abnormality patterns across all the clinical states. Intra-imaging modalities results show also a significant correspondence between the MCM's outcome and the reference data, supporting the effectiveness of this model to capture factor-specific features during disease progression. See Videos S1-S5 for 3D illustrations of the reconstructed multifactorial dynamic alterations. Also, based on the predicted relative disease progression scores among the different LOAD clinical sub-stages (EMCI, LMCI, LOAD), the results suggest that LOAD development occurs during a large pathological temporal process. In a continuous disease progression scale of [0, 1], with 0 corresponding to the initial pathological onset and 1 to the LOAD diagnosis, EMCI and LMCI symptoms appear around the 0.55 and 0.91 positions, respectively.

Finally, we evaluated the MCM's predictive power on new instances of data. For this, first we used the multifactorial alteration patterns of the subjects at EMCI and LMCI states to predict the future trajectories of the data, fitting the model with only these two states and projecting the alteration pattern at the time that a hypothetical subject should reach the LOAD stage. The results (Fig. 3a) confirm a strong predictive accuracy, explaining 74.83% (P < 0.0001) of LOAD's characteristic multifactorial variance. Also, we tested the model's capacity to predict intermediary stages of disease progression, training it with the subjects at EMCI and LOAD states and predicting the characteristic LMCI alteration patterns. We observed again a strong predictive power (Fig. 3b), with the MCM explaining 84.50% (P < 0.0001) of the observed variance for subjects diagnosed as LMCI. To conclude, we evaluated the model's capacity to predict the past trajectories of the data, fitting the model with the subjects at the LMCI and LOAD states and predicting (via backward integration) the multifactorial alteration patterns for the EMCI subjects. In line with previous results, the MCM significantly explained the alteration data observed for the EMCI subjects (Fig. 3c), explaining around 52% (P < 0.0001) of its total variance. All together, these findings (Figs. 3a-c) suggest that the proposed MCM may be a precise diagnostic tool of future brain disorganization and cognitive properties, which can contribute to clarify early and intermediate processes associated to disease progression. In addition, even when our analyses are based on a population-based sample, these results support the spatiotemporal continuity of the EMCI, LMCI and LOAD stages.

*Identifying potential triggering events in LOAD*

Vascular dysregulation, Aβ toxicity, metabolic impairment, neuronal hyperactivity, and accelerated tissue neurodegeneration are among
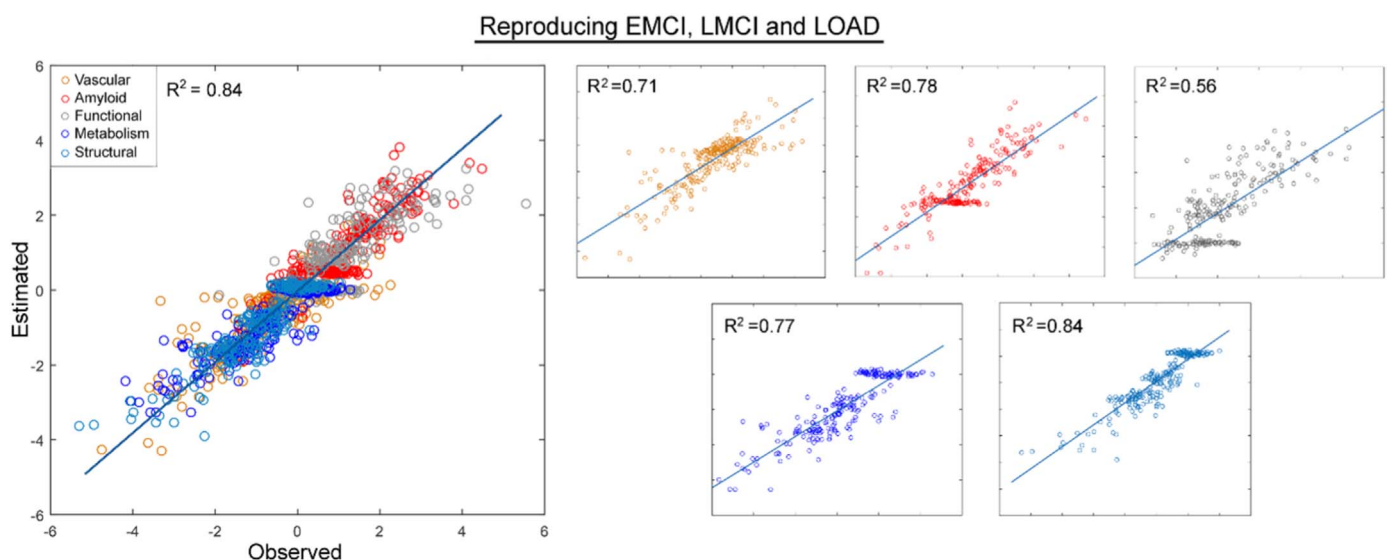


**Fig. 2.** Reconstruction and prediction of the multifactorial alteration patterns in LOAD progression. Estimated vs. observed values for EMCI, LMCI and LOAD, starting from a HC state. Each point represents a brain region; colors correspond to different imaging modalities. See also Videos S1–S5.
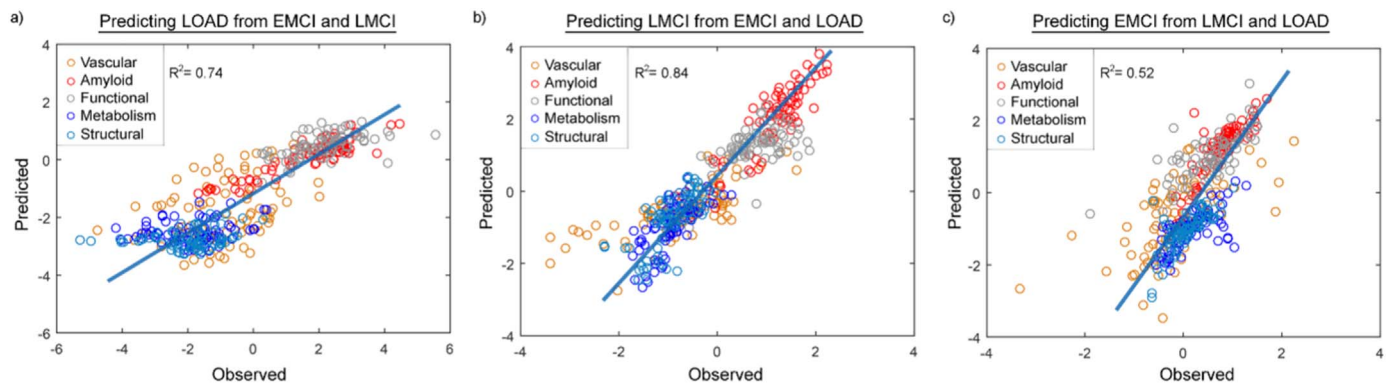
**Fig. 3.** Prediction on new instances of data (cross-validation analysis). a) Predicted vs. observed LOAD alteration values, training the model only with EMCI and LMCI states. b) Predicted vs. observed LMCI alteration values, training only with EMCI and LOAD states. c) Predicted vs. observed EMCI alteration values, training only with LMCI and LOAD states.

the basic mechanisms of the most consistent/polemic hypotheses of LOAD, which are still the subject of continuing scientific debate (Iturria-Medina et al., 2016). It is still unknown which of these or other pathological factors may trigger the disease process, as well as how the multifactorial pathological signals propagate concurrently from the initial affected regions to connected brain areas. The introduced MCM model allowed us to evaluate quantitatively different cascade hypotheses by the data-driven identification of the brain areas where the disease starts and the specific associated factor(s) that become abnormal. In practical terms, every time the model is evaluated it starts from an initial non-zero condition $S(t_0)$ (see *Methods*). This is equivalent to introducing a perturbation in the defined brain system, assumed to be until that time in a steady state equilibrium, with the subsequent purpose of predicting any future time point by using the model's analytic formulations (expressions (5) and (13)). Usually, this perturbation tends to be small in magnitude (i.e. with a few regions/factors presenting non-zero values), reflecting the fact that neurodegeneration constitutes a long-term process, starting years before the brain's multifactorial alterations and the associated clinical symptoms are detectable with current techniques. For the hypothetical case of studying brain concussion effects, the initial perturbation should not be necessarily small, but proportional to the received impact. For obtaining a plausible initial condition and optimizing the model's biological parameters, we used a fully automated algorithm (Text S2), estimating the most-likely factors/regions and parameters that better explain the multivariate alteration patterns observed in the data. The estimation included an intrinsic cross-validation, generating 10 training/test disjoint folds, which allowed us to obtain the initial condition that

maximized the predictive power of the model. In addition, a bootstrapping procedure, generating 500 repetitions with replacement, was used to characterize the biological and methodological stability of the results. Subsequently, for each of the five biological factors considered, we obtained the probability of being the initial macroscopic triggering event in LOAD. This probability was calculated as the relative number of times, across all the bootstrapping repetitions, that a given factor was identified as the initial pathological event (see *Most-likely disease triggering events and regional epicenters* subsubsection, expressions (15) and (16), *Methods*). Similarly, for each brain region, we computed its probability to be a disease spatial epicenter (see expressions (17) and (18), *Methods*).

Comparing the five factors considered, we observed a significant predominance of the vascular and functional dysregulation components as the most-likely initial pathological events (Fig. 4a). The vascular factor was automatically identified as the triggering LOAD cause for 58.66% of all the model evaluations/repetitions. It was followed, as possible initial pathological event, by functional dysregulation (40.58%), glucose metabolism impairment (0.32%), Aβ deposition/propagation (0.21%) and structural degeneration (0.21%). In addition, the model identified the left hippocampus, left and right entorhinal cortex, left putamen, left temporal regions and the right hippocampus as the most-likely regional disease epicenters (Fig. 4b). These regions have been historically associated with the genesis of LOAD, being among the earliest areas targeted by the disease (Braak and Del Tredici, 2015; Braak, 1991; Khan et al., 2014). See *Discussion* section for subsequent analysis/interpretation.
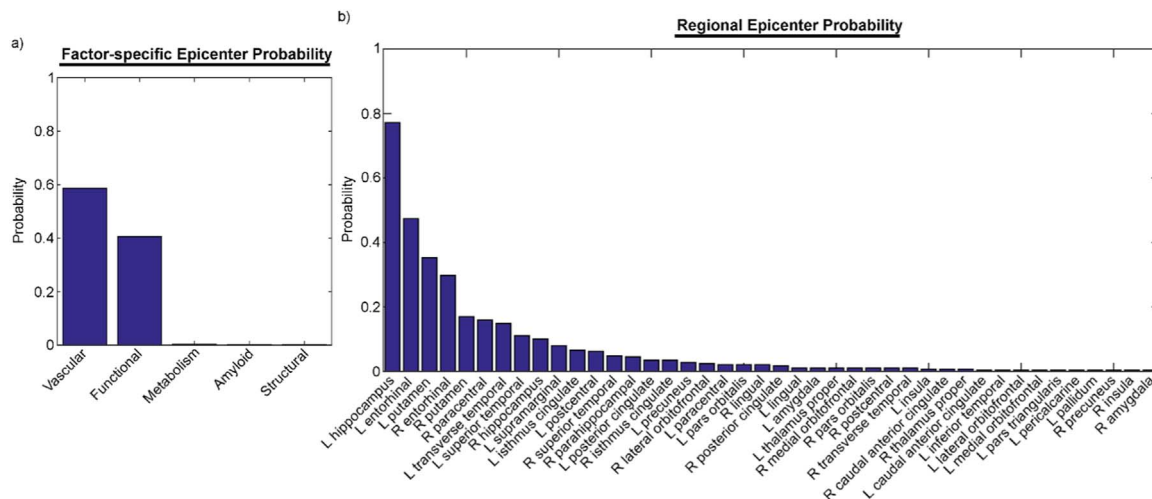


**Fig. 4.** Most-likely causal epicenters for LOAD. a) Factor-specific probability for triggering LOAD. b) Multifactorial regional relevance on disease onset. Regions were sorted according to their total estimated participation probability on the disease onset. Regions with zero participation probability are not included.
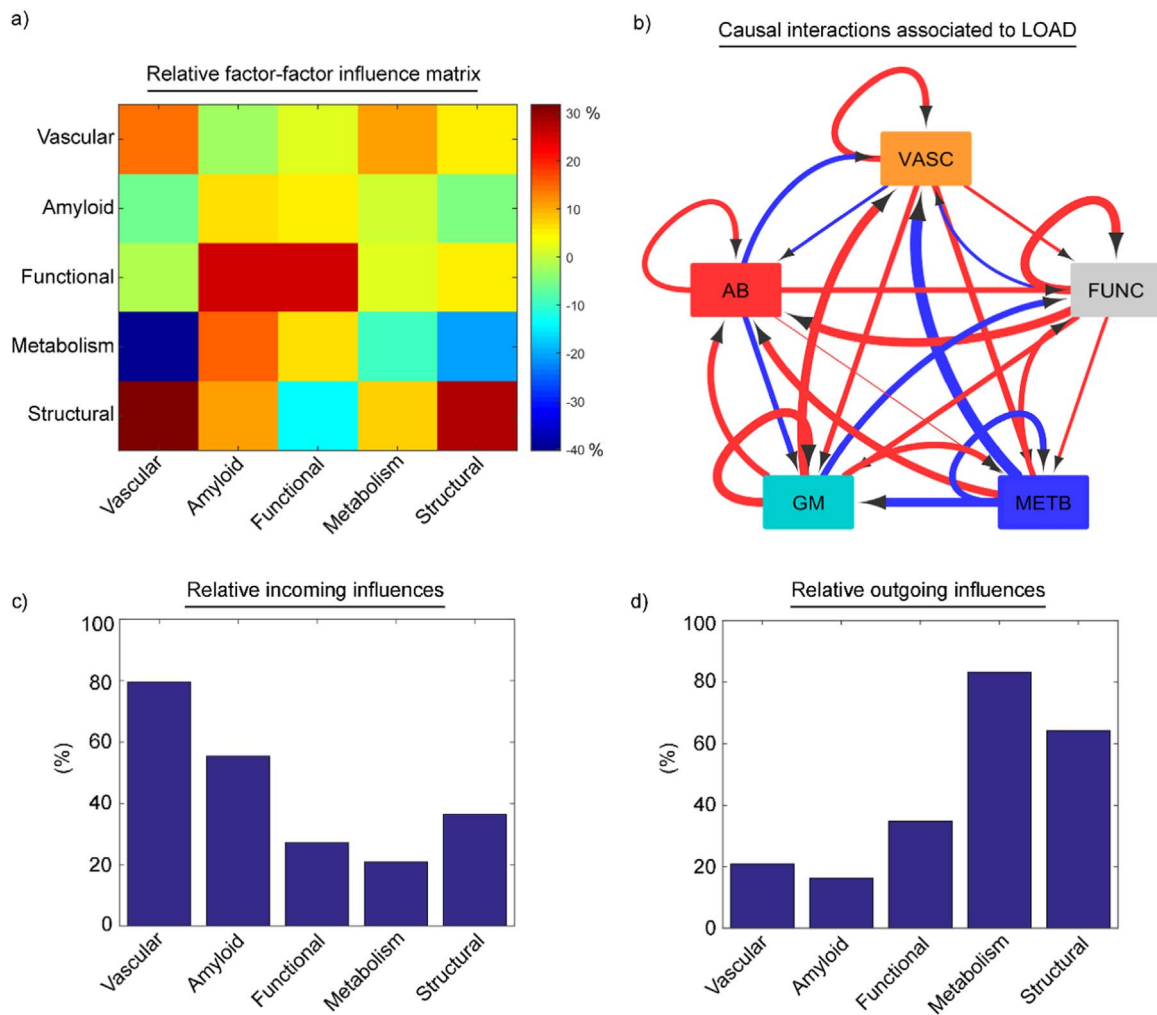
**Fig. 5.** Direct interactions associated to LOAD progression (population-based results). a) Relative factor-factor influence matrix. Element (*n,m*) reflects the percent of regional changes in the factor *m* that are caused by the direct influence of the factor *n*. See also Table S2 for obtained values. b) Associated causal diagram. Red and blue links correspond to positive and negative direct relations, respectively. c) Relative incoming influences. d) Relative outgoing influences.

*Characterizing direct factor-factor interactions and intra-brain propagation properties*

As mentioned, the direct coupling among multiple biological factors is a key feature of the brain, both in health and disease (Andreone et al., 2015; Bero et al., 2011; Iturria-Medina and Evans, 2015; Qosa et al., 2014; Readnower et al., 2011; Šišková et al., 2014). The identification of the triggering events associated to a given disorder is not enough for understanding its progression, but it is also crucial to identify the underlying complex interacting mechanisms. Here, we used the MCM to estimate and characterize the direct factor-factor associations characteristic of the whole HC to LOAD transition. The *relative factor-factor influence* metric allowed us to quantify the percent of regional changes in a given biological factor that are caused by the direct influence of any other factor (see *Interpreting factor-factor direct interactions and alteration spread* subsection, *Methods*).

Fig. 5a-b illustrate the obtained population-based direct associations (see also Table S2 for obtained values). The results suggest that the vascular supply has a strong positive impact on glucose metabolism and itself, explaining around 10.66% and 14.39% of the observed alterations in these factors, respectively. On the contrary, and consistently with the fact that vascular dysregulation modulates Aβ clearance (Qosa et al., 2014), the results support a negative impact of vascular dysregulation on Aβ deposition (−3.21%). In a feedback mechanism, we also observed a negative impact of Aβ accumulation on vascular integrity (-5.88%), in agreement with the experimental evidence suggesting that Aβ induces morphological and architectural vasculature changes, resulting in altered CBF (Meyer et al., 2008). In addition, Aβ burden influences negatively gray matter density (-4.65%) and increases functional activity at rest (4.99%, i.e. more Aβ binding implying an increase in functional hyperactivity and vice versa, as reported by Buckner et al. (2009)). Consistently, functional activity dysregulation presented a strong direct impact on Aβ deposition (25.82%), as suggested by Yuan and Grutzendler (2016). The results suggest also a strong functional self-loop (25.87%), being the functional alterations at rest mostly explained by intrinsic functional mechanisms and the grey matter density changes (-13.77%). The latter interaction is in line with the fact that neuronal structural degeneration can trigger functional hyperexcitability and associated network dysfunctions (Šišková et al., 2014). Glucose metabolism presents the strongest of all the analyzed direct interactions, negatively impacting the vascular properties (-40%). As proposed in the *Discussion* section, this strong negative link may be reflecting a crucial compensatory mechanism (i.e. the increasing failing in glucose metabolism, characteristic of LOAD progression, may provoke an increasing and futile demand of blood supply, in order to get more and more glucose, which paradoxically is less and less metabolized as the disease progresses). As expected, we observed an strong positive link also among glucose metabolism and grey matter density (28.30%). The energy production impairment can directly affect the neuronal/glial demands, conducing to cell dysfunc-

tion, injury, and death (Demetrius and Driver, 2013).

Next, we analyzed how much each specific biological factor is directly influenced by the others. For this we calculated the *relative incoming influences* (Fig. 5c), which reflects the percent of the regional changes in each factor that is caused by the direct influences of all other considered biological factors, excluding self-effects (see *Interpreting factor-factor direct interactions and alteration spread* subsection, *Methods*). The results suggest that the vascular component is the most influenced factor, with around 80% of its alterations directly caused by multifactorial effects. In particular, intra-brain vascular changes are strongly modulated by glucose metabolism and structural alterations (40% and 32%, respectively). The high incoming connectivity degree of the vascular system could be making it particularly vulnerable to pathologic alterations (see *Discussion* section). Aβ was identified as the second most influenced biological factor, with around 58% of its alterations directly caused by multifactorial effects. Functional hyperactivity and glucose metabolism dysregulation presented the strongest impacts on Aβ, explaining around 25% and 15% of the observed Aβ increase, respectively. As debated in the *Discussion* section, the observed high levels of direct influences on vascular and Aβ properties may be reflecting the high vulnerability and susceptibility of these biological factors, which could explain why they have been historically reported as very early pathological events during LOAD progression.

Complementary to the previous analysis, by means of the *relative outcoming influence* measure (see *Interpreting factor-factor direct interactions and alteration spread* subsection, *Methods*), we quantified the percent of the regional changes in all the considered biological factors that are caused by the direct influence of each specific biological factor. Our results (Fig. 5d), based on the five biological factors considered, suggest that once that the initial triggering events occurs, the provoked glucose metabolism impairment becomes the most directly influential factor. It has a strong influence on the other four considered factors, particularly on the vascular and structural components. Structural degeneration is the second most influential factor, also with a notable impact on vascular flow (31.69%). See the *Discussion* section for further interpretation.

In addition to factor-factor interactions, the propagation of factor-specific alterations is thought to be a relevant mechanism on disease progression (Cabral et al., 2012; Friston et al., 2014; Iturria-Medina et al., 2014; Iturria-Medina and Evans, 2015; Sanz Leon et al., 2013). Fig. 6a-b present the average vascular and anatomical connectomes reconstructed in this study, which constituted the main physical substrates through which the simulated factor-specific alterations propagated. We observed that the vascular network presents a considerably higher presence of inter-hemispheric connections than the structural network. Despite this difference, a Mantel test with permu-
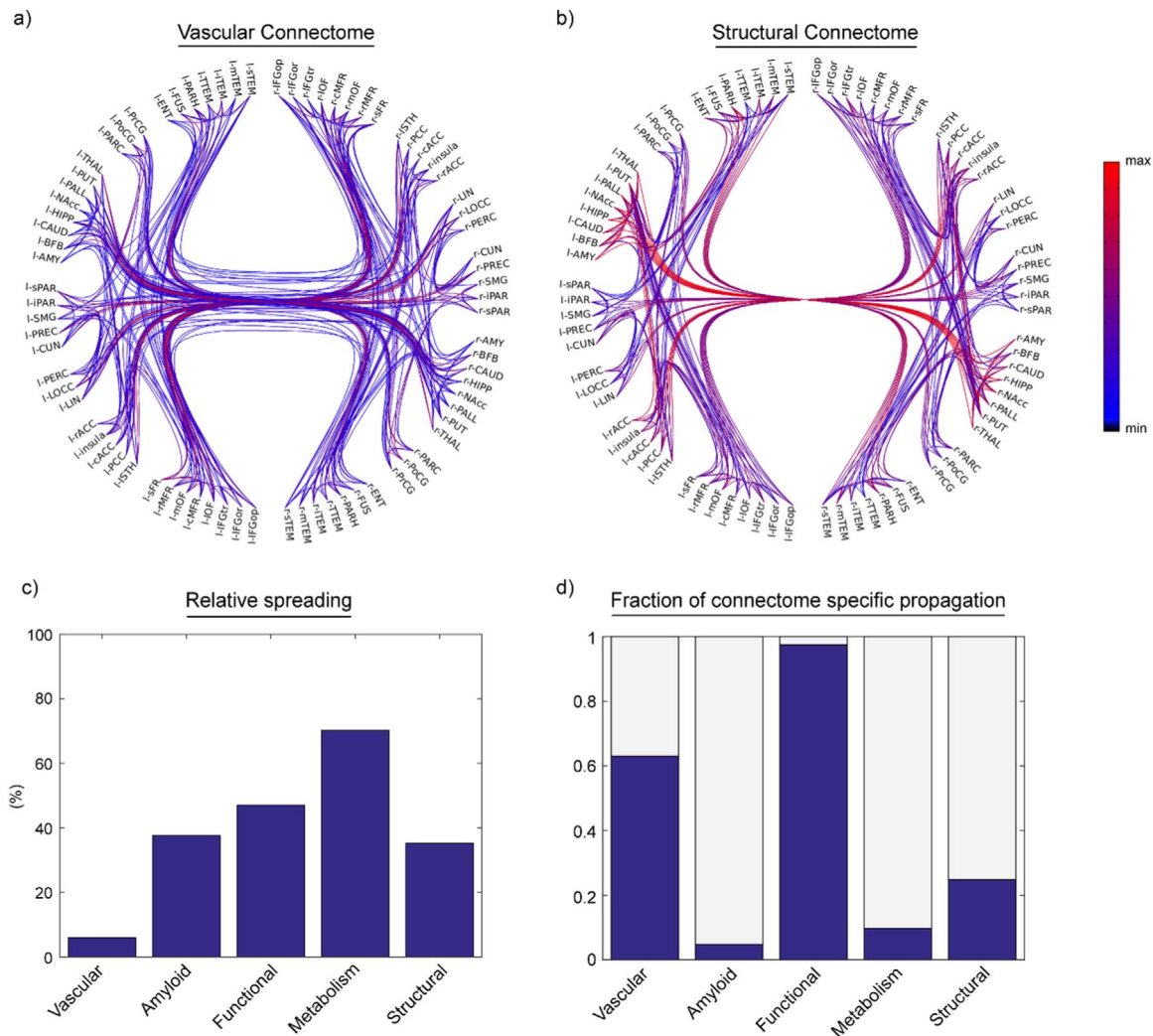


**Fig. 6.** Multifactorial intra-brain propagation mechanisms in LOAD. a) Reconstructed vascular connectome. b) Reconstructed anatomical connectome. Both a) and b) correspond to the averages across all the clinical groups. A significant similarity between both networks was confirmed by a Mantel test with permutations (R=0.58, P < 0.0001). c) *Relative spreading* (*Diff*; see *Methods*), reflecting the percent of the regional changes in each factor that are caused by the factor's spreading through the brain's physical connections. d) Fraction of the aberrant propagation in (c) that spread through the vascular or the anatomical networks, indicated by blue or light gray bars, respectively. For complete regions names, see Table S3.

tations confirmed the significant similarity among both networks (R=0.58, P < 0.0001). This similarity might be explained by the fact that during the initial neurodevelopmental processes, axon-guidance cues mediate the navigation of blood vessels along predestined tracks (Zacchigna et al., 2008), whereas angiogenic vascular endothelial growth factor regulates the migration of various neuron types to their final destination (Schwarz and et al., 2004; Zacchigna et al., 2008). Next, we evaluated the *relative spreading* of each factor, which reflects the percent of changes in a given factor that are not caused by local multifactorial interactions but by interregional spreading through physical connections. Among the five biological factors, metabolic and functional impairment presented the highest relative propagation tendencies (Fig. 6c), which propagation effects explaining around a 70% and 50% of the changes in these factors. As analyzed in the *Discussion* section, these findings may be associated to cortical depression spreading (CSD) and hyperactivity dispersion effects, which are key processes in neurodegeneration (Chang et al., 2013; de Haan et al., 2012; Mergenthaler et al., 2013). We also observed a strong propagation tendency of Aβ and structural alterations, which may be reflecting prion-like mechanisms (Brundin et al., 2010; Frost and Diamond, 2010) and axonal degeneration effects (Lingor et al., 2012). In addition, according to the results, while glucose metabolic dysregulations, Aβ and structural alterations tend to propagate following the route of structural connections (Fig. 6d), functional and vascular impairments may propagate mostly by vascular connections.

### Identifying optimum therapeutic strategies for stopping and reversing LOAD progression

The ultimate goal of an effective therapeutic strategy is to prevent and/or reverse brain multifactorial abnormalities and undesired symptoms associated with disease progression/severity. In the specific case of LOAD, and other dementias, this goal translates into stopping, and ideally reversing, cognitive deterioration, which also guarantees a normal multifactorial reorganization of the brain's properties. In terms of control theory (Kalman, 1963; Klickstein et al., 2016; Liu et al., 2011), an *output control strategy* (*Methods*, Eq. (6)) applied to the multifactorial causal network obtained here can help to identify the optimum therapeutic strategy to modify the individual cognitive/behavioral state, without necessarily restoring all the affected brain properties. On the other hand, a *full control strategy* (*Methods*, Eq. (8)) can focus on restoring to clinically normal ranges all the considered biological properties, consequently influencing the cognitive/behavioral output. Motivated by this, here we aimed to: i) investigate the feasibility of an *output control* vs a *full control* therapeutic strategy to effectively control LOAD progression, and ii) for each strategy, to identify the most practical LOAD intervention, considering either all possible single-factor or combinatorial treatments.

For each considered biological factor or combination of factors (up to a maximum of five), we estimated the theoretical optimum input signal and corresponding cost-energy to conduce the cognitive state or the brain's state space (Fig. 1b) from a hypothetical LOAD state to a HC clinical state (see *Methods*). Fig. 7 shows the controlled brain state space and cognitive trajectories, for both the *output control* (Fig. 7a) and the *full control* (Fig. 7b) strategies. Interestingly, we observed that both controlling strategies conduce to the recovering of the cognitive state at the POST-T point, suggesting that with an appropriate treatment it is possible to stop and reverse LOAD's cognitive severity. However, although an *output control strategy* (Fig. 7a) was conducive to cognitive improvement, it is far from controlling the regional alterations observed in all the intra-brain biological factors, which in fact will continue growing with time. As commented in the *Discussion* section (*Applications on the design and evaluation of therapeutic interventions* subsection), this finding suggests that, although extensively practiced in the pharmaceutical and clinical fields, a LOAD
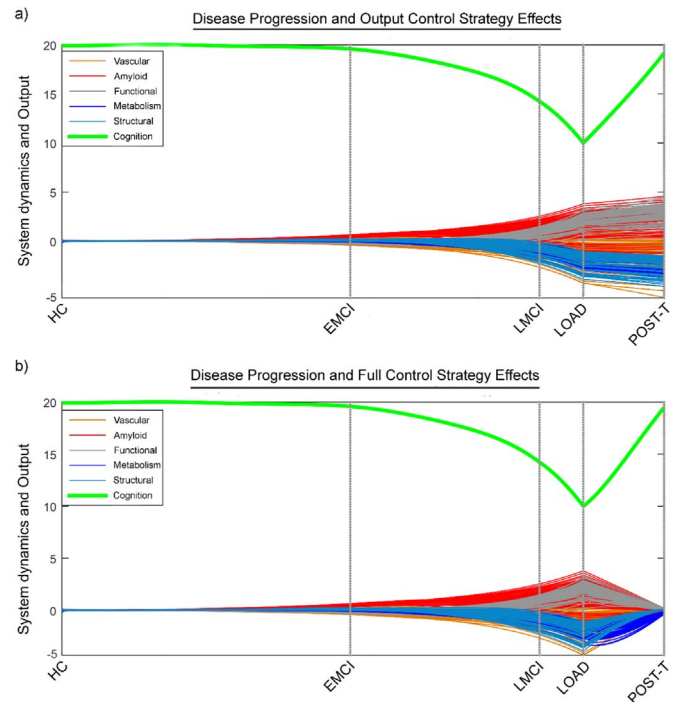


**Fig. 7.** Controlled brain and cognitive trajectories for a hypothetic HC to LOAD to HC transition. a) Effects of using an *output control strategy*, with the unique goal to stop/reverse the cognitive deterioration. b) Effects of using a *full control strategy*, where the overall goal is to normalize the brain's multifactorial properties, indirectly influencing the cognitive state. For each case, results correspond to the minimum cost-energy strategy identified across all possible factor-specific treatments (see Fig. 6a-b). Each line represents the alteration level of a brain region/factor (zero value implying normal equilibrium), with the exception of the cognitive variable (MMSE, green line), which is at its original scale. For visualization purposes, in (a) and (b) the cognitive variable was rescaled to the range [10-20]. See also Videos S1–S5.

therapy selected uniquely because of its capacity to restore cognition (or decline/stops its deterioration) may still be conducing to abnormal brain states, characterized by other unstopped or newly generated (e.g. secondary) effects. On the contrary, a *full control strategy* (Fig. 7b) can ideally conduce to both the recuperation of cognition and the normalization of the brain's multifactorial properties, although this may be at the expense of increasing the required cost-energy levels (Fig. 8a-b). See Videos S1-S5 for 3D representations of the reconstructed multifactorial dynamic alterations.

The control cost-energy is a theoretical measure of deformation, reflecting how much the system must be altered to reach a desired final state (see *Methods*). In practical terms, the more expensive a control intervention, the more difficult will be to implement. It will require the input of therapeutic signals with an extremely strong biological impact, which will be difficult to achieve and could have strong undesired secondary effects. Here, when we analyzed the theoretical ordering in cost-energy requirements for all possible factors-specific interventions, we observed considerably lower cost-energy values for combinatorial than for single-target treatments (Fig. 8a-b). In particular, for the *full control* strategy, our results suggest that the combination of the five biological factors considered would provide an efficient and effective treatment to reverse LOAD effects, ideally conducing to a clinically normal state. Interestingly, for both control strategies, treatments targeting only the Aβ propagation/deposition required high amounts of interventional energy, and consequently would require a large application time to achieve a positive therapeutic impact (see also Fig. S1). Finally, we repeated the previous controllability analyses for the hypothetical case in which it is only desired to stop the disease's progression, i.e. halting memory deterioration and the increase in multifactorial brain alterations, without necessarily reversing the
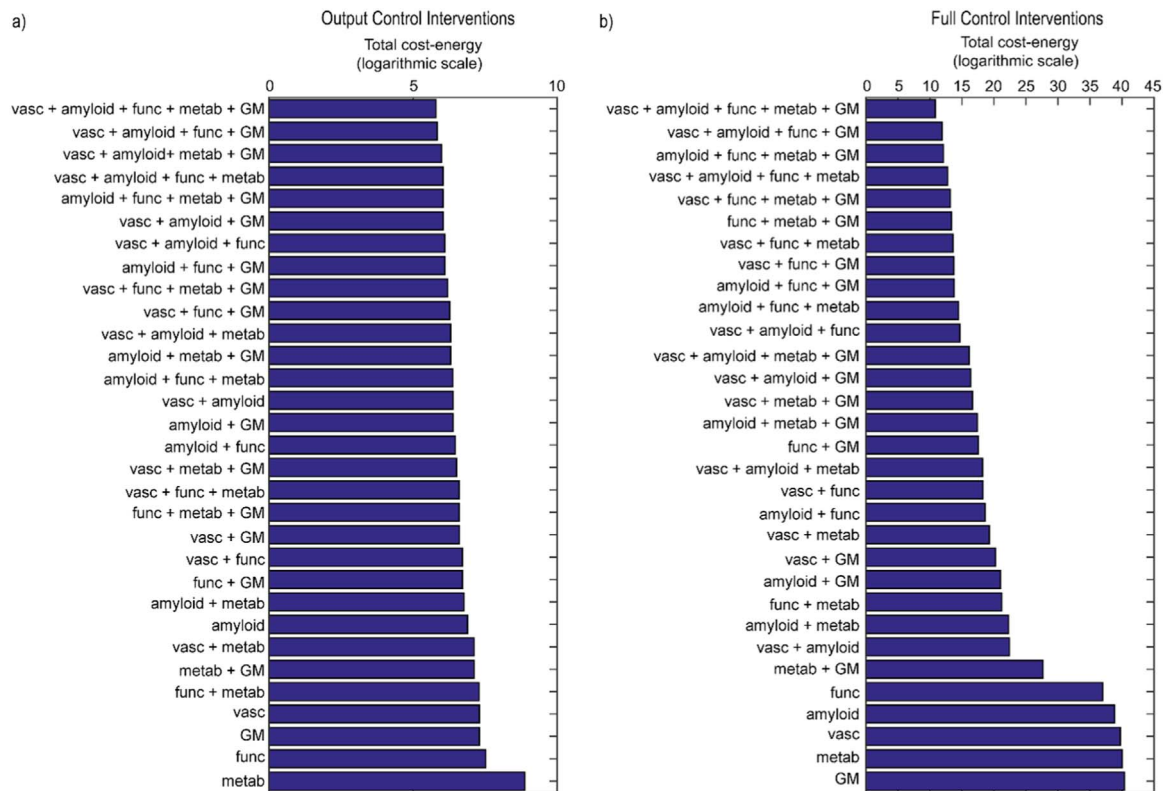
**Fig. 8.** Optimum cost-energies of hypothetical LOAD therapeutic strategies. a) *Output control strategy* and b) *full control strategy* costs. Single-target and combinatorial (up to a maximum of five target factors) therapies were sorted from minimum to maximum energy required to reverse disease progression, from an advanced LOAD state to a normal HC state. Notice that, for both strategies, targeting only Aβ is among the most biologically expensive alternatives (see also Figs. S1–S2).

disease's pathological effects. Fig. S2 shows the theoretical ordering obtained in cost-energy requirements for stopping the pathological progression at the EMCI state. We observed equivalent results, i.e. a more consistent result of a *full control strategy* over an *output control strategy*, with a considerable reduction of post-treatment effects, and considerably lower cost-energy values for combinatorial than for single-target interventions.

See *Discussion* section (*Applications on the design and evaluation of therapeutic interventions* subsection) for further analysis/interpretation.

## Discussion

In this study we sought to solve three major challenges of current neurological research: i) no characterization of direct multifactorial biological interactions, ii) no consideration of the concurrent spreading of multiple pathological effects across physical brain networks, and iii) an inability to predict in advance the effects of multifactorial interventional strategies. We overcome these methodological issues by means of a multifactorial causal model of brain (dis)organization and cognition. This, in addition to clarifying disease-specific pathological mechanisms, allows the evaluation of the biological feasibility of single-target or combinatorial therapies. Applied to the study of LOAD progression, our model offers for the first time an integrative causal description of this disorder and, remarkably, quantitative guidelines for stopping/reversing LOAD-associated multifactorial/cognitive deterioration.

### Towards a multifactorial interpretation of brain disorders

Recently, we showed the importance of considering large amounts of multiple/concomitant biomarkers instead than only a priori selected biomarkers, as well the advantages of using data-driven instead of

observational models for the understanding of neurodegenerative disorders (Iturria-Medina et al., 2016). However, similarly to many other disease progression models (Donohue et al., 2014; Dukart et al., 2013; Jack et al., 2013; Young et al., 2014), our previous analysis was still based on changes in magnitude of the different biological factors, as a measure of factor relevance on the disease. We highlighted, although without solving it, the issue that small initial alterations in specific biological factors can cause large alterations in other interconnected factors (Iturria-Medina et al., 2016). In this sense, only causal analyses can potentially lead us to a more integrated understanding of pathological progression, clarifying the intrinsic brain multifactorial pathological interactions that take place at different spatiotemporal scales. The MCM introduced here attempts to address this central point. Notice that causality is intrinsic in the differential equations that define this model. Similarly to previous causal models (Friston et al., 2014; Stephan et al., 2010; Valdes-sosa et al., 2011b), but now going beyond the unifactor interaction/spreading, the MCM equations describe: (i) how the present state of a given biological factor, at a given brain region, causes new fluctuations in other factors or itself at the same region or at a different brain region, via multifactorial local interactions or by spreading through brain connections, and (ii) how the system's dynamic may change by the influence of external inputs (e.g. cognitive/sensory stimulus, therapeutic interventions or environmental influences). By estimating the most-likely initial triggering causal effects and the direct interactions weights among pairs of multiple relevant biological factors, it would then be possible to recover the multifactorial chronological stages that lead to the outcome of a complex disease. This concept/method might have profound implications on the ways in which we study brain disorders, i.e. focusing on the discovery and interpretation of multifactorial causal mechanisms instead of in the traditional observation of magnitude changes.

In particular, our results suggest that a vascular disequilibrium is the most-likely macroscopic triggering event leading to LOAD devel-

opment (Fig. 4). This finding led to a crucial question: what makes the vascular system particularly vulnerable at the point of being a very early pathologic event? When analyzing the factor-factor links that define the complex dynamic of the brain system during LOAD progression, we found that the vascular system is the most influenced component by the other considered biological factors (Fig. 5c). According to our data/results, around 80% of the observed vascular alterations may be explained by local multifactorial interactions. This may reflect the continuous high vascular vulnerability to fluctuations in other factors. Consequently, the lifetime convergence of multifactorial fluctuations on the vascular system may make it particularly fragile, which might explain why it is a potential early pathologic event on dementia progression. Interestingly, the fact that other (i.e. non-vascular) factors have a non-zero probability to start/trigger the disease process (Fig. 4a) might imply that, although less likely, different multifactorial alterations can lead to the disease's observed alteration patterns/symptoms. We attribute this possibility to the existence of factor-factor causal mechanisms (see Fig. 5 and next paragraph). Once a given initial alteration or a combination of them occurs at the identified most-likely epicenter regions (Fig. 4), the brain's intrinsic/invariant factor-factor causal mechanisms and interregional spreading capacity guarantee that this alteration will eventually impact the other biological factors and regions, initiating a pathological cascade of events that under particular conditions (e.g. genetic, life style, environment) may conduce to LOAD. It is, however, essential to consider that the initial causal/triggering disease factor (or combination of factors) may not be necessarily be detected by current imaging/statistical techniques as a "significant" abnormality. The proposed MCM and its associated analysis/results are incompatible with the traditional binary/dichotomized classification among "negative" or "positive" subjects with regard a given pathologic biomarker (see Jack et al., 2016, 2015). Such "negative" vs "positive" separation ignores the fact that small, scarcely statistically detectable, changes in a given biological factor can have strong temporal impacts on disease progression, affecting in time other brain factors, which could reach accentuated/notable magnitude changes. Consequently, the traditional binary classification procedures could have been leading to wrong causal biological interpretations, suggesting for example that a given pathological condition (e.g. Aβ accumulation/propagation) appears/acts negatively before others just because it is more readily statistically detectable (Jack et al., 2016, 2015).

However, despite the relevance of identifying potential initial pathologic events, the finding of multiple consistent factor-factor interactions evidences the indispensable role of complex multifactorial interactions on disease development. An interesting example is the futile increase in CBF that a glucose metabolic dysfunction may induce. Our results (Fig. 5a-b and Table S2) suggest that alterations in glucose metabolism have a strong impact on vascular properties, explaining around -40% of the changes on it. We attribute the negative link to a compensatory mechanism: the increasing failing in glucose metabolism, characteristic of LOAD progression, may provoke an increasing demand of blood supply, in order to obtain more glucose. Due to the metabolic dysfunction, the arriving glucose is less used with disease progression, making futile the biological efforts to guarantee a higher CBF, in a continuous aberrant cycle. We also observed an strong positive link among glucose metabolism and grey matter density, in line with the fact that the energy production impairment can directly affect the neuronal/glial demands, conducing to cell dysfunction, injury and death (Demetrius and Driver, 2013). As expected, we observed a negative impact of vascular dysregulation on Aβ deposition, consistent with the fact that vascular dysregulation modulates Aβ clearance (Qosa et al., 2014). At the same time, Aβ accumulation presented a negative impact on vascular integrity, which is in line with the experimental evidence suggesting that Aβ induces morphological and architectural vasculature changes (Meyer et al., 2008). In line with previous studies, the results suggest that Aβ burden and functional activity at rest

modulate directly each other (Buckner et al., 2009; de Haan et al., 2012; Yuan and Grutzendler, 2016), with more Aβ accumulation during disease progression associated to hyperactivity increase, and vice versa. We also observed a strong impact of grey matter density alterations on functional activity, in agreement with the experimental evidence supporting that neuronal structural degeneration can trigger functional hyperexcitability and associated network dysfunction (Šišková et al., 2014). Factor-factor interactions are concurrent with the intra-brain spreading of factor-specific alteration effects. In line with the general point of view, pathologic changes appearing in the initial epicenter regions (Fig. 4b) may propagate to other regions, spreading the disease via physical connections (Fig. 6a-b). However, our results (Fig. 6c) suggest that, in addition to the conventional functional and Aβ changes propagation (Brundin et al., 2010; de Haan et al., 2012; Frost and Diamond, 2010), other biological factors may propagate their pathologic effects also to distant brain regions. Glucose metabolic impairment and structural degeneration presented high interregional propagation effects, with CSD (Chang et al., 2013; Mergenthaler et al., 2013) and axonal degeneration (Lingor et al., 2012) being potential underlying mechanisms, respectively. Although needing further investigation, in general these multifactorial propagation results may be evidencing the methodological importance of considering other intra-brain disease spreading mechanisms associated to LOAD, beyond the classically studied functional and Aβ dispersions.

Altogether, our results suggest that LOAD it is not caused by a unique dominant biological factor (e.g. vascular dysregulation, Aβ, or metabolic dysfunction, etc.) but by the complex interplay among multiple relevant factors, which interact continuously across the lifetime, from before the initial pathologic event to the final/advance disease stages. We believe that this characteristic is not unique of LOAD, but a major attribute of multiple brain disorders. Subsequent studies, from our or other groups, should explore the multifactorial causal attribute of prevalent brain diseases. In order to help achieve this goal, we anticipate that the used programming source code and implementation experience will be shared relatively soon, with the additional goal of promoting/supporting *open science*.

*Applications on the design and evaluation of therapeutic interventions*

An essential application of considering multifactorial direct interactions and their impact on cognition is the possibility of predicting the cascade of effects that a given external input may cause in the brain. In this sense, generative quantitative models constitute a natural *in silico* scenario to design and evaluate the effects of treatments. Here we quantified, for the first time to the best of our knowledge, the impact that multiple combinatorial or single-target interventions may have on the brain and its immediate output, cognition. The principles of control theory (Kalman, 1963; Klickstein et al., 2016; Liu et al., 2011), in combination with the formulated MCM, allow us to evaluate not only the theoretical impact of each possible therapeutic strategy but also to quantify its feasibility, in terms of control energy required to direct the system to the desired state (e.g. a clinically normal state, in the neurological context). For each hypothetical intervention, the obtained control energy can be interpreted as the accumulation of deformation (in the same scale that the state space variables) that is necessary to apply to the system in order to conduce it to the desired state. Although these values have been calculated here for hypothetical interventions, mathematically it is straightforward to calculate the real effects that a given therapy may have over the brain and its immediate outputs, cognition/behaviour. For characterizing an actual intervention of interest, it would be only necessary to have longitudinal data associated to it, including also the precise information about the time points of the intervention (for defining a scaled input signal, $u(t)$, see expression (5)) and at least some a priori knowledge of the brain regions that should be directly affected (for defining the input matrix, $B$, see expression (5)). With a few mathematical operations, it would be then possible to

identify a direct function, translating treatment characteristics to brain and cognitive/clinical impacts. In consequence, the introduced methodology can be particularly useful for comparing alternative interventions (Figs. 7, 8 and Fig. S1–S2) and identifying optimum pharmacological strategies to prevent and/or reverse disease progression.

Although still requiring further exploration at the individual level (see *Limitations and future work* subsection), the population-based results obtained here motivate two main comments. First, we observed that although an *output control strategy* (i.e. the basic goal is to modify the individual cognitive/behavioral state, without restoring the affected brain properties; Fig. 7a) was conducive to cognitive improvement, it is far from controlling the regional alterations observed in all the intra-brain biological factors. Regularly practiced in the pharmaceutical and clinical fields, this strategy is strongly susceptible to the appearance of negative secondary effects. After the intervention, the remaining brain alterations can continue interacting locally, via factor-factor direct interactions, and can also continue to spread to other brain regions, where other factor-factor interactions can take place. A *full control strategy* (i.e. the basic goal is to modify/restore the affected brain properties; see Fig. 7b and Videos S1-S5) can ideally conduce to both the normalization of the brain's multifactorial properties and consequently to the recuperation of cognition. However, it is not always clear what can be classified as a post-treatment remaining alteration or if it could trigger a negative secondary cascade. As defined in the *Methods* section, the MCM proposes to characterize each brain variable according to its alteration/disequilibrium level or dissimilarity/distance to an initial pathology-free state. Assuming an endpoint state, which could be the same initial pathology-free state or other proposed by the clinician, the model can be used to identify the optimum theoretical intervention to reach such state. One possibility may be to conduce the individual brain to reach similar properties before progressing on the disease, but usually the associated data is not available, particularly for extended neurodegenerative processes. Alternatively, the values observed for demographically-matched clinically normal subjects can be assumed as endpoints. But it is still under scientific debate what is ideal or clinically normal, and that may even change from person to person. In this sense, the MCM could also contribute to the evaluation of the individual impact of multiple possible endpoints, even before a given treatment is designed and applied. The simulation of future trajectories, beyond each candidate endpoint, may be useful to clarify if an associated (optimum) intervention would be eventually conducing to an acceptable or to an undesired cognitively/clinically condition. Second, we observed considerably lower cost-energy values for combinatorial than for single-target interventions (Fig. 8a-b). This supports the previously postulated advantage of using combinatorial over single-target treatments (Sun et al., 2013). According to our results, the combination of multiple biological factors as targets would provide an efficient and effective treatment to reverse LOAD effects, ideally conducing to a clinically normal state. Treatments targeting only the Aβ propagation/deposition required high amounts of interventional energy (see Fig. S1), which might explain why recent one-target Aβ based therapies have failed to improve clinical outcomes in LOAD (Doody et al., 2014; Salloway et al., 2014). We observed similar results for the hypothetical case in which it is only desired to stop the disease's progression (see Fig. S2), i.e. halting memory deterioration and the increase in multifactorial brain alterations, without necessarily reversing the disease's pathological effects. The latter indicates that similar therapeutic principles are valid for preventing or reversing the disease.

In summary, we believe that the proposed model may be particularly useful for: i) comparing multiple possible intervention strategies, in terms of effectiveness and biological costs, ii) defining feasible endpoints, designed also to avoid negative secondary brain effects, and iii) evaluating additional practical information associated to treatments decisions (e.g. technical difficulties and/or associated economic costs), which would contribute to obtaining a realistic tradeoff among theoretical predictions and relevant practical factors. In line with the latter application, it is important to keep in mind that any result based on this methodology should be considered in combination with the practical clinical feasibility associated with each possible treatment. For example, targeting only four of the considered factors, e.g. excluding grey matter density as a target, requires more control energy than targeting the five considered factors together (Fig. 8a-b). But the former intervention may be still more practical in clinical terms, due to the therapeutic difficulty in promoting grey matter density increase (or neurogenesis) across the whole brain. Thus, if we expect this controlling methodology and others similar (Betzel et al., 2016; Freund et al., 2016; Muldoon et al., 2016) to represent a turning point for the assisted design of disease-specific therapeutics, it will be critical to establish a strong compromise among theoretical predictions and clinical feasibility. Potentially, incorporating a priori penalty weights on the cost-energy function (expression (9)), may be useful for integrating the theoretical estimations with the available information about technical and/or economic difficulties for implementing a given therapy. These methodological extensions will be among the main focuses of our subsequent studies.

*Limitations and future work*

Brain modeling techniques strongly depend on how precisely the considered descriptors reflect specific biological/pathophysiological processes. The biological parameters estimated with the MCM are not exempt from this dependency. In particular, the data used in this study present some key limitations. First, although the MCM has been explicitly formulated to consider the case of individual trajectories, the lack of subjects with all imaging modalities required us to fit the data on all samples, explaining and/or predicting population-based disease stage patterns. Consequently, all the results/conclusions presented here are only representative of the average tendency in the ADNI population, and do not necessarily explain all possible individual mechanisms. However, this optimization limitation does not alter the causality nature of the model, intrinsic in the differential equations that define it. The fact that multiple of the obtained factor-factor relationships are in line with previously reported interactions, based on experimental analyses, supports the biological validity of our population-based findings. Importantly, we are already extending the model formulation to deal with missing data, predicting the specific missing modalities, which will allow us to fit individual datasets and analyze/report consistencies and dissimilarities between population-based and individual-based results. The extended formulation, and associated individual-based results, will be the main focus of a subsequent publication. Second, and for the same reason, continuous changes in brain connectivity were approximated by inter-group changes. Despite this, notice that the proposed model is not restricted to linear dynamics. The causal multifactorial network A(t) can change dynamically, depending on the alterations of the structural and vascular connectomes. In the case of presenting continuous connectivity information (e.g. for longitudinal individual datasets), expressions (4) and (5) can be accurately evaluated using advanced integration methods (Carbonell et al., 2008), while the corresponding controllability analysis can be performed using non-linear approaches (Wang et al., 2016). Third, due to the lack of young clinically normal subjects and to large longitudinal datasets, it is difficult to define a reference healthy pattern. We used age and gender-matched clinically normal subjects, which could have already non-pathological aging affectations, and/or also an intrinsic predisposition to not develop LOAD. Thus, we may be comparing the unhealthy subjects with "special" individuals. Consequently, this may be affecting the precision of the abnormality/disequilibrium measures. Fourth, we used approximate methods to reconstruct vascular and anatomical brain connectomes. Fig. 6 illustrates the (dis)similarities among both obtained connectomes. Further formulations/analyses should explore the possibility of making the MCM robust to the choice of connectomes reconstruction algorithms,

in order to reduce this potential source of bias (see (Huynh-Thu et al., 2010; Iturria-Medina, 2013)). Fifth, our main analyses were based on a specific brain parcellation scheme (Klein and Tourville, 2012). Although this parcellation improved the consistency and accuracy of labeling human cortical areas, the use of different parcellation schemes can impact differently brain network reconstruction results (Zalesky et al., 2010), and could potentially affect also the quantification of the multimodal regional patterns. Notably, in a preliminary analysis, we obtained consistent results using a different parcellation (AAL atlas), considering 90 cortical and subcortical areas covering all the brain´s gray matter (Tzourio-Mazoyer et al., 2002). For the AAL parcellation, the results suggest once more that a vascular dysregulation may be the most-likely initial pathologic event leading to LOAD. The vascular factor was automatically identified as the triggering LOAD cause for around the 66% of all the model evaluations/repetitions, and was followed by functional dysregulation (27%) and amyloid deposition (7%). We also observed a significant similarity among the obtained multifactorial interaction measures for both parcellations (Pearson correlation: $R=0.7$, $P < 0.0001$). We are already extending this analysis by performing a broad model exploration/validation using multiple parcellation schemes, defined at different spatial scales, with the ultimate goal of making the MCM-based conclusions robust to the choice of parcellation. Sixth, for the sake of simplicity on model formulation and evaluation, in this study we used a linear function for modeling the multifactorial regional impacts on cognition. In principle, any other function could be used, depending on how robustly it can be estimated previously from the available data. When considering different function alternatives for the system's output function, it will be important to reach an appropriate trade-off between accuracy and complexity. For example, although the inclusion of region-region interactions would benefit the model's accuracy, it would also increase considerably the number of parameters to be estimated. This would not be necessarily a problem if it is used a relative large sample size, although could be needed the use of feature selection techniques. Other alternative could be the use of kernel or radial basis functions, which would be useful to capture non-linear effects. Seventh, here multifactorial brain alterations were only evaluated in the grey matter, ignoring possible alterations within the white matter and other LOAD-relevant areas (e.g. CSF, arachnoid and pia matter/space). The inclusion of other tissues and brain areas will be on the focus of other MCM-based separate studies, for which we will combine structural white matter alterations (evaluated with T1, T2 FLAIR, diffusion-weighted connectivity measurements (Iturria-Medina, 2013)), white matter vascular integrity, CSF ventricles volume and density, extra-brain space measurements, among others. This multivariate information can be readily inserted into the flexible formulation of the MCM, ideally conducing to an advance spatiotemporal description/representation of the brain's multifactorial nature.

## Data availability

All data used in this study is available at the Alzheimer's Disease Neuroimaging Initiative (ADNI) database (adni.loni.usc.edu).

## Author contributions

ADNI acquired the data. YIM conceived the model/study, implemented the programming source code, preprocessed and analyzed the data, and wrote the manuscript. FMC provided continuous feedback on the model definition, source code implementation, data analysis and the manuscript preparation/writing. FC constructed Fig. 6a-b. ACE and RCS revised/corrected the manuscript. All authors contributed to constructive discussions regarding the interpretation of the results.

## Conflict of interest

The authors declare no competing financial interest.

## Acknowledgments

## Appendix A. Supplementary material

Supplementary data associated with this article can be found in the online version at doi:10.1016/j.neuroimage.2017.02.058.

## References

Andreone, B.J., Lacoste, B., Gu, C., 2015. Neuronal and vascular interactions. Neurosci. Res. 38, 25–46. http://dx.doi.org/10.1146/annurev-neuro-071714-033835.

Ashburner, J., 2007. A fast diffeomorphic image registration algorithm. Neuroimage 38, 95–113.

Bero, A.W., Yan, P., Roh, J.H., Cirrito, J.R., Stewart, F.R., Raichle, M.E., Lee, J., Holtzman, D.M., 2011. Neuronal Activity Regulates the Regional Vulnerability to Amyloid- b Deposition, vol. 14, pp. 5–7. ⟨http://doi.org/10.1038/nn.2801⟩.

Betzel, R.F., Gu, S., Medaglia, J.D., Pasqualetti, F., Bassett, D.S., 2016. Optimally Controlling the Human Connectome: the Role of Network Topology. pp. 1–23.

Braak, H., Del Tredici, K., 2015. The preclinical phase of the pathological process underlying sporadic Alzheimer's disease. Brain 138, 2814–2833. http://dx.doi.org/10.1093/brain/awv236.

Braak, H., B.E, 1991. Neuropathological stageing of Alzheimer-related changes. Acta Neuropathol. 82, 239–259.

Brundin, P., Melki, R., Kopito, R., 2010. Prion-like transmission of protein aggregates in neurodegenerative diseases. Nat. Rev. 11, 301–307.

Buckner, R.L., Sepulcre, J., Talukdar, T., Krienen, F.M., Liu, H., Hedden, T., Andrews-Hanna, J.R., Sperling, R.A., Johnson, K.A., 2009. Cortical hubs revealed by intrinsic functional connectivity: mapping, assessment of stability, and relation to Alzheimer's disease. J. Neurosci. 29, 1860–1873. http://dx.doi.org/10.1523/JNEUROSCI.5062-08.2009.

Cabral, J., Hugues, E., Kringelbach, M.L., Deco, G., 2012. Modeling the outcome of structural disconnection on resting-state functional connectivity. Neuroimage. http://dx.doi.org/10.1016/j.neuroimage.2012.06.007.

Carbonell, F., Jimenez, J., Pedroso, L., 2008. Computing multiple integrals involving matrix exponentials. J. Comput. Appl. Math. 213, 300–305.

Chang, J.C., Brennan, K.C., He, D., Huang, H., Miura, R.M., Wilson, P.L., Wylie, J.J., 2013. A mathematical model of the metabolic and perfusion effects on cortical

spreading depression. PLoS One 8, 1–9. http://dx.doi.org/10.1371/journal.pone.0070469.

Chao-Gan, Y., Yu-Feng, Z., 2010. DPARSF: a MATLAB toolbox for "Pipeline" data analysis of resting-state fMRI. Front. Syst. Neurosci. 4, 13. http://dx.doi.org/10.3389/fnsys.2010.00013.

Chen-Plotkin, A.S., 2014. Unbiased approaches to biomarker discovery in neurodegenerative diseases. Neuron 84, 594–607. http://dx.doi.org/10.1016/j.neuron.2014.10.031.

Coleman, T.F., Li, Y., 1996. An interior trust region approach for nonlinear minimization subject to bounds. SIAM J. Optim. 6, 418–445. http://dx.doi.org/10.1137/0806023.

Coleman, T.F., Li, Y., 1992. On the convergence of reflective newton methods for large-scale nonlinear minimization subject to bounds. Math. Program., 1–36.

Crossley, N.A., Mechelli, A., Scott, J., Carletti, F., Fox, P.T., Mcguire, P., Bullmore, E.T., 2014. The hubs of the human connectome are generally implicated in the anatomy of brain disorders. Brain 137, 2382–2395. http://dx.doi.org/10.1093/brain/awu132.

de Haan, W., Mott, K., van Straaten, E.C.W., Scheltens, P., Stam, C.J., 2012. Activity dependent degeneration explains hub vulnerability in Alzheimer's disease. PLoS Comput. Biol. 8, e1002582. http://dx.doi.org/10.1371/journal.pcbi.1002582.

Demetrius, L.A., Driver, J., 2013. Alzheimer's as a metabolic disease. Biogerontology 14, 641–649.

Donohue, M.C., Jacqmin-Gadda, H., Le Goff, M., Thomas, R.G., Raman, R., Gamst, A.C., Beckett, L.A., Jack, C.R., Weiner, M.W., Dartigues, J.-F., Aisen, P.S., 2014. Estimating long-term multivariate progression from short-term data. Alzheimer's Dement 10, S400–S410. http://dx.doi.org/10.1016/j.jalz.2013.10.003.

Doody, R.S., Thomas, R.G., Farlow, M., Iwatsubo, T., Vellas, B., Joffe, S., Kieburtz, K., Raman, R., Sun, X., Aisen, P.S., Siemers, E., Liu-Seifert, H., Mohs, R., 2014. Phase 3 trials of solanezumab for mild-to-moderate Alzheimer's disease. N. Engl. J. Med. 370, 311–321. http://dx.doi.org/10.1056/NEJMoa1312889.

Dukart, J., Kherif, F., Mueller, K., Adaszewski, S., Schroeter, M.L., Frackowiak, R.S.J., Draganski, B., Neuroimaging, D., 2013. Generative FDG-PET and MRI Model of Aging and Disease Progression in Alzheimer's Disease, vol. 9, pp. 1–11. ⟨http://doi.org/10.1371/journal.pcbi.1002987⟩.

Evans, A., 2013. Networks of anatomical covariance. Neuroimage 80, 489–504.

Evans, A., Kamber, M., Collins, D., Macdonald, D., 1994. An MRI-based probabilistic atlas of neuroanatomy. In: Shorvon, S., Fish, D., Andermann, F., Bydder, G., Stefan, H. (Eds.), Magnetic Resonance Scanning Epilepsy. Plenum, New York, 263–274.

Fonteijn, H.M., Modat, M., Clarkson, M.J., Barnes, J., Lehmann, M., Hobbs, N.Z., Scahill, R.I., Tabrizi, S.J., Ourselin, S., Fox, N.C., Alexander, D.C., 2012. An event-based model for disease progression and its application in familial Alzheimer's disease and Huntington's disease. Neuroimage, 1–10. http://dx.doi.org/10.1016/j.neuroimage.2012.01.062.

Freund, P., Friston, K., Thompson, A.J., Stephan, K.E., Ashburner, J., Bach, D.R., Nagy, Z., Helms, G., Draganski, B., Mohammadi, S., Schwab, M.E., Curt, A., Weiskopf, N., 2016. Embodied neurology: an integrative framework for neurological disorders Embodied neurology : anintegrative framework for neurological disorders. Brain 139, 1855–1861. http://dx.doi.org/10.1093/brain/aww076.

Friston, K.J., Kahan, J., Biswal, B., Razi, A., 2014. A DCM for resting state fMRI. Neuroimage 94, 396–407. http://dx.doi.org/10.1016/j.neuroimage.2013.12.009.

Frost, B., Diamond, M.I., 2010. Prion-like mechanisms in neurodegenerative diseases. Nat. Rev. Neurosci. 11, 155–159. http://dx.doi.org/10.1038/nrn2786.

Gao, J., Liu, Y.-Y., D'Souza, R.M., Barabási, A.-L., 2014. Target control of complex networks. Nat. Commun. 5, 5415. http://dx.doi.org/10.1038/ncomms6415.

Huynh-Thu, V.A., Irrthum, A., Wehenkel, L., Geurts, P., 2010. Inferring regulatory networks from expression data using tree-based methods. PLoS One 5, 1–10. http://dx.doi.org/10.1371/journal.pone.0012776.

Iadecola, C., 2004. Neurovascular regulation in the normal brain and in Alzheimer's disease. Nat. Rev. Neurosci. 5, 347–360.

Iturria-Medina, Y., 2013. Anatomical brain networks on the prediction of abnormal brain states. Brain Connect., 1–41.

Iturria-Medina, Y., Canales-Rodríguez, E.J., Melie-García, L., Valdés-Hernández, P.A., Martínez-Montes, E., Alemán-Gómez, Y., Sánchez-Bornot, J.M., 2007. Characterizing brain anatomical connections using diffusion weighted MRI and graph theory. Neuroimage 36, 645–660. http://dx.doi.org/10.1016/j.neuroimage.2007.02.012.

Iturria-Medina, Y., Evans, A.C., 2015. On the central role of brain connectivity in neurodegenerative disease progression. Front. Aging Neurosci. 7, 90. http://dx.doi.org/10.3389/fnagi.2015.00090.

Iturria-Medina, Y., Sotero, R.C., Toussaint, P.J., Evans, A.C., 2014. Epidemic spreading model to characterize misfolded proteins propagation in aging and associated neurodegenerative disorders. PLoS Comput. Biol. 10, e1003956. http://dx.doi.org/10.1371/journal.pcbi.1003956.

Iturria-Medina, Y., Sotero, R.C., Toussaint, P.J., Mateos-Perez, J.M., Evans, A.C., ADNI, 2016. Early role of vascular dysregulation on late-onset Alzheimer's disease based on multifactorial data-driven analysis. Nat. Commun. 7, 11934. http://dx.doi.org/10.1038/ncomms11934.

Jack, C.R., Knopman, D.S., Chételat, G., Dickson, D., Fagan, A.M., Frisoni, G.B., Jagust, W., Mormino, E.C., Villemagne, V.L., Visser, P.J., Vos, S.J.B., 2016. Suspected non-Alzheimer disease pathophysiology — concept and controversy. Nat. Publ. Gr., 1–8. http://dx.doi.org/10.1038/nrneurol.2015.251.

Jack, C.R., Knopman, D.S., Jagust, W.J., Petersen, R.C., Weiner, M.W., Aisen, P.S., Shaw, L.M., Vemuri, P., Wiste, H.J., Weigand, S.D., Lesnick, T.G., Pankratz, V.S., Donohue, M.C., Trojanowski, J.Q., 2013. Tracking pathophysiological processes in Alzheimer's disease: an updated hypothetical model of dynamic biomarkers. Lancet Neurol. 12, 207–216. http://dx.doi.org/10.1016/S1474-4422(12)70291-0.

Jack, C.R., Wiste, H.J., Weigand, S.D., Knopman, D.S., Mielke, M.M., Vemuri, P., Lowe, V., Senjem, M.L., Gunter, J.L., Reyes, D., Machulda, M.M., Roberts, R., Petersen, R.

C., 2015. Different Definitions of Neurodegeneration Produce Similar Amyloid/neurodegeneration Biomarker Group Findings, pp. 1–13. ⟨http://doi.org/10.1093/brain/awv283⟩.

Jack, C.R., Jr, Knopman, D.S., Jagust, W.J., et al., 2010. Hypothetical model of dynamic biomarkers of the Alzheimer's pathological cascade. Lancet Neurol. 9, 119–128.

Jagust, W., Bandy, D., Chen, K., Foster, N., Landau, S., Mathis, C., Al, E., 2010. The Alzheimer's disease neuroimaging initiative positron emission tomography core. Alzheimers Dement 6, 221–229.

Kailah, T., 1980. Linear Systems. Prentice-Hall, New Jersey.

Kalman, R., 1963. Mathematical description of linear dynamical systems. J. Soc. Ind. Appl. Math. Ser. A 1, 152–192.

Khan, U. a, Liu, L., Provenzano, F. a, Berman, D.E., Profaci, C.P., Sloan, R., Mayeux, R., Duff, K.E., Small, S. a, 2014. Molecular drivers and cortical spread of lateral entorhinal cortex dysfunction in preclinical Alzheimer's disease. Nat. Neurosci. 17, 304–311. http://dx.doi.org/10.1038/nn.3606.

Klein, A., Tourville, J., 2012. 101 labeled brain images and a consistent human cortical labeling protocol. Front. Neurosci. 6, 171. http://dx.doi.org/10.3389/fnins.2012.00171.

Klickstein, I.S., Shirin, A., Sorrentino, F., 2016. Optimal Target Control of Complex Networks.

Klupp, E., Förster, S., Grimmer, T., Tahmasian, M., Yakushev, I., Sorg, C., Yousefi, B.H., Drzezga, A., 2014. In Alzheimer's disease, hypometabolism in low-amyloid brain regions may be a functional consequence of pathologies in connected brain regions. Brain Connect 4, 371–383. http://dx.doi.org/10.1089/brain.2013.0212.

Lingor, P., Koch, J.C., Tönges, L., Bähr, M., 2012. Axonal degeneration as a therapeutic target in the CNS. Cell Tissue Res. 349, 289–311. http://dx.doi.org/10.1007/s00441-012-1362-3.

Liu, Y.-Y., Slotine, J.-J., Barabási, A.-L., 2011. Controllability of complex networks. Nature 473, 167–173. http://dx.doi.org/10.1038/nature10011.

Mergenthaler, P., Lindauer, U., Dienel, G., Meisel, A., 2013. Sugar for the brain: the role of glucose in physiological and pathological brain function. Trends Neurosci. 36, 587–597. http://dx.doi.org/10.1016/j.tins.2013.07.001.Sugar.

Meyer, E.P., Ulmann-Schuler, A., Staufenbiel, M., Krucker, T., 2008. Altered morphology and 3D architecture of brain vasculature in a mouse model for Alzheimer's disease. Proc. Natl. Acad. Sci. USA 105, 3587–3592. http://dx.doi.org/10.1073/pnas.0709788105.

Mišić, B., Betzel, R.F., Nematzadeh, A., Goñi, J., Griffa, A., Hagmann, P., Flammini, A., Ahn, Y.Y., Sporns, O., 2015. Cooperative and competitive spreading dynamics on the human connectome. Neuron 86, 1518–1529. http://dx.doi.org/10.1016/j.neuron.2015.05.035.

Monti, R.P., Hellyer, P., Sharp, D., Leech, R., Anagnostopoulos, C., Montana, G., 2014. Estimating time-varying brain connectivity networks from functional MRI time series. Neuroimage 103, 427–443. http://dx.doi.org/10.1016/j.neuroimage.2014.07.033.

Muldoon, S.F., Pasqualetti, F., Gu, S., Cieslak, M., Grafton, S.T., Vettel, J.M., Bassett, D. S., 2016. Stimulation-Based Control of Dynamic Brain Networks, vol. 54.

Qosa, H., Abuasal, B.S., Romero, I.A., Weksler, B., Couraud, P.-O., Keller, J.N., Kaddoumi, A., 2014. Differences in Amyloid-β Clearance Across Mouse and Human Blood–brain Barrier Models.pdf.

Raj, A., Kuceyeski, A., Weiner, M., 2012. A network diffusion model of disease progression in dementia. Neuron 73, 1204–1215. http://dx.doi.org/10.1016/j.neuron.2011.12.040.

Readnower, R., Sauerbeck, A., Sullivan, P., 2011. Mitochondria, Amyloid β, and Alzheimer's Disease.pdf. ⟨http://doi.org/10.4061/2011/104545⟩.

Rubinov, M., Sporns, O., 2010. NeuroImage Complex network measures of brain connectivity: uses and interpretations. Neuroimage 52, 1059–1069. http://dx.doi.org/10.1016/j.neuroimage.2009.10.003.

Salloway, S., Sperling, R., Fox, N.C., Blennow, K., Klunk, W., Raskind, M., Sabbagh, M., Honig, L.S., Porsteinsson, A.P., Ferris, S., Reichert, M., Ketter, N., Nejadnik, B., Guenzler, V., Miloslavsky, M., Wang, D., Lu, Y., Lull, J., Tudor, I.C., Liu, E., Grundman, M., Yuen, E., Black, R., Brashear, H.R., 2014. Two phase 3 trials of bapineuzumab in mild-to-moderate Alzheimer's disease. N. Engl. J. Med. 370, 322–333. http://dx.doi.org/10.1056/NEJMoa1304839.

Sanz Leon, P., Knock, S. a, Woodman, M.M., Domide, L., Mersmann, J., McIntosh, A.R., Jirsa, V., 2013. The Virtual Brain: a simulator of primate brain network dynamics. Front. Neuroinform. 7, 10. http://dx.doi.org/10.3389/fninf.2013.00010.

Sanz-Leon, P., Knock, S. a, Spiegler, A., Jirsa, V.K., 2015. Mathematical framework for large-scale brain network modelling in The Virtual Brain. Neuroimage. http://dx.doi.org/10.1016/j.neuroimage.2015.01.002.

Schwarz, Q., et al., 2004. Vascular endothelial growth factor controls neuronal migration and cooperates with Sema3A to pattern distinct compartments of the facial nerve. Genes Dev. 18, 2822–2834.

Sheikh, S., Haque, E., Mir, S., 2012. Neurodegenerative diseases: multifactorial conformational diseases and their therapeutic interventions. J. Neurodegener. Dis. 2013, 8. http://dx.doi.org/10.1155/2013/563481/.

Šišková, Z., Justus, D., Kaneko, H., Friedrichs, D., Henneberg, N., Beutel, T., Pitsch, J., Schoch, S., Becker, A., VonderKammer, H., Remy, S., 2014. Dendritic structural degeneration is functionally linked to cellular hyperexcitability in a mouse model of alzheimer's disease. Neuron 84, 1023–1033. http://dx.doi.org/10.1016/j.neuron.2014.10.024.

Sled, J.G., Zijdenbos, A.P., Evans, A.C., 1998. A Nonparametric Method for Automatic Correction of Intensity Nonuniformity in MRI Data, vol. 17, pp. 87–97.

Sotero, R.C., Trujillo-Barreto, N.J., Iturria-Medina, Y., Carbonell, F., Jimenez, J.C., 2007. Realistically coupled neural mass models can generate EEG rhythms. Neural Comput..

Stam, C.J., van Straaten, E.C.W., Van Dellen, E., Tewarie, P., Gong, G., Hillebrand, A.,

Meier, J., Van Mieghem, P., 2016. The relation between structural and functional connectivity patterns in complex brain networks. Int. J. Psychophysiol. 103, 149–160. http://dx.doi.org/10.1016/j.ijpsycho.2015.02.011.

Stephan, K.E., Penny, W.D., Moran, R.J., den Ouden, H.E.M., Daunizeau, J., Friston, K.J., 2010. Ten simple rules for dynamic causal modeling. Neuroimage 49, 3099–3109. http://dx.doi.org/10.1016/j.neuroimage.2009.11.015.

Street, J.O., Carroll, R.J., Ruppert, D., 1988. A note on computing robust regression estimates via iteratively reweighted least squares. Am. Stat. 42, 152–154.

Sun, X., Vilar, S., Tatonetti, N.P., 2013. High-throughput methods for combinatorial drug discovery. Sci. Transl. Med. 5. http://dx.doi.org/10.1126/scitranslmed.3006667.

Tibshirani, R., 1996. Regression Selection and Shrinkage via the Lasso. J. R. Stat. Soc. B. http://dx.doi.org/10.2307/2346178.

Tournier, J.D., Yeh, C.H., Calamante, F., Cho, K.H., Connelly, A., Lin, C.P., 2008. Resolving crossing fibres using constrained spherical deconvolution: validation using diffusion-weighted imaging phantom data. Neuroimage 42, 617–625. http://dx.doi.org/10.1016/j.neuroimage.2008.05.002.

Trujillo-Ortiz, A., Hernandez-Walls, R., Castro-Perez, A., Barba-Rojo, K., 2006. MOUTLIER1: Detection of Outlier in Multivariate Samples Test. A MATLAB file [WWW Doc].

Tzourio-Mazoyer, N., Landeau, B., Papathanassiou, D., Crivello, F., Etard, O., Delcroix, N., Mazoyer, B., Joliot, M., 2002. Automated anatomical labeling of activations in SPM using a macroscopic anatomical parcellation of the MNI MRI single-subject brain. Neuroimage 15, 273–289. http://dx.doi.org/10.1006/nimg.2001.0978.

Valdes-sosa, P.A., Roebroeck, A., Daunizeau, J., Friston, K., 2011a. NeuroImage Effective connectivity: influence, causality and biophysical modeling. Neuroimage, 1. http://dx.doi.org/10.1016/j.neuroimage.2011.03.058.

Valdes-sosa, P.A., Roebroeck, A., Daunizeau, J., Friston, K., 2011b. NeuroImage Effective connectivity: influence, causality and biophysical modeling. Neuroimage 58, 339–361. http://dx.doi.org/10.1016/j.neuroimage.2011.03.058.

van den Heuvel, M.P., Hulshoff Pol, H.E., 2010. Exploring the brain network: a review on resting-state fMRI functional connectivity. Eur. Neuropsychopharmacol. 20, 519–534. http://dx.doi.org/10.1016/j.euroneuro.2010.03.008.

WHO, 2016. World Health Statistics 2016: monitoring health for the SDGs. Sustainable Development Goals. (doi:ISBN 978 92 4 156526 4).

Wilks, S., 1966. Multivariate statistical outliers. Sankhya Ser. A 25, 407–426.

Wu, J.W., Hussaini, S.A., Bastille, I.M., Rodriguez, G.A., Mrejeru, A., Rilett, K., Sanders, D.W., Cook, C., Fu, H., Boonen, R.A.C.M., Herman, M., Nahmani, E., Emrani, S., Figueroa, Y.H., Diamond, M.I., Clelland, C.L., Wray, S., Duff, K.E., 2016. Neuronal activity enhances tau propagation and tau pathology in vivo. Nat. Neurosci.. http://dx.doi.org/10.1038/nn.4328.

Young, A.L., Oxtoby, N.P., Daga, P., Cash, D.M., Fox, N.C., Ourselin, S., Schott, J.M., Alexander, D.C., 2014. A data-driven model of biomarker changes in sporadic Alzheimer's disease. Brain 137, 2564–2577. http://dx.doi.org/10.1093/brain/awu176.

Yuan, P., Grutzendler, J., 2016. Attenuation of -amyloid deposition and neurotoxicity by chemogenetic modulation of neural activity. J. Neurosci. 36, 632–641. http://dx.doi.org/10.1523/JNEUROSCI.2531-15.2016.

Zacchigna, S., Lambrechts, D., Carmeliet, P., 2008. Neurovascular signalling defects in neurodegeneration. Nat. Rev. Neurosci. 9, 169–181. http://dx.doi.org/10.1038/nrn2336.

Zalesky, A., Fornito, A., Harding, I.H., Cocchi, L., Yücel, M., Pantelis, C., Bullmore, E.T., 2010. Whole-brain anatomical networks: does the choice of nodes matter? Neuroimage 50, 970–983.

Zang, Y., Jiang, T., Lu, Y., He, Y., Tian, L., 2004. Regional homogeneity approach to fMRI data analysis. Neuroimage 22, 394–400. http://dx.doi.org/10.1016/j.neuroimage.2003.12.030.

Zlokovic, B.V., 2011. Neurovascular pathways to neurodegeneration in Alzheimer's disease and other disorders. Nat. Rev. Neurosci. 12, 723–738. http://dx.doi.org/10.1038/nrn3114.

Zou, Q.-H., Zhu, C.-Z., Yang, Y., Zuo, X.-N., Long, X.-Y., Cao, Q.-J., Wang, Y.-F., Zang, Y.-F., 2008. An improved approach to detection of amplitude of low-frequency fluctuation (ALFF) for resting-state fMRI: fractional ALFF. J. Neurosci. Methods 172, 137–141. http://dx.doi.org/10.1016/j.jneumeth.2008.04.012.